(NASA-CR-175899) [ACTIVITIES OF THE SOLID STATE PHYSICS RESEARCH INSTITUTE] Annual Report, 1 Jan. - 31 Dec. 1984 (Virginia State Univ., Petersburg.) 55 p
HC A05/MF A01
CSCL 20L G3/76

N85-28818
THRU
N85-28821
Unclas
15093

ANNUAL REPORT

SOLID STATE PHYSICS RESEARCH INSTITUTE

Virginia State University
Petersburg, VA 23803

Supported by NASA Grant NAG 1-476

Report Period: 1/1/84-12/31/84

Annual Report
Solid State Physics Research Institute
Virginia State University
Petersburg, VA 23803

Supported by NASA Grant NAG 1-416
Report Period: 1/1/84 - 12/31/84

The Solid State Physics Research Institute at Virginia State University was formally organized in January 1984 subsequent to the funding received through NASA grant NAG 1-416. The institute is a collection of three research programs. Two of these, muon spin rotation studies and studies of annealing problems in gallium arsenide, were previously funded by NASA through separate grants. The MuSR program was begun in 1972, while the GaAs studies were initiated in 1982. A third program, Hall effect studies in semiconductors, was initiated with the establishment of the institute. C. E. Stronach is director of the institute as well as P/I of the MuSR program. J. J. Stith and J. C. Davenport (VSU physics department chairman) are co-principal investigators of the GaAs program, while G. W. Henderson is P/I of the Hall effect program.

The purposes of this institute are threefold: (1) to perform state-of-the-art research in both basic and applied aspects of solid state physics which is both intrinsically interesting and which can be applied to problems of interest to NASA; (2) to develop a self-sustaining physics research program at VSU which will bring distinction to the University and its physics department; and (3) to provide training and experiences to students which will prepare them for careers in research.

The following sections describe the activities of each of the research programs during the period January 1 - December 31, 1984. Following this is a section describing activities which do not fall strictly within any of the three

programs, plus descriptions of student activities, equipment acquisitions, and future plans.

Muon Spin Rotation Studies

The bulk of the muon spin rotation research work centered around the development of the muon spin rotation facility at the Alternating Gradient Synchrotron (AGS) of Brookhaven National Laboratory (BNL). A previous run had taken place in May 1983, in which the initial beam development had taken place, along with studies of muon diffusion in aluminum-copper alloys. However, the need for substantial upgrading of the system, plus a move of the apparatus to another location on the beam line, made substantial development work necessary. The VSU participants concentrated on designing and fabricating the collimation system, which is shown in figure 1. This improved collimation system, plus improvements in detectors (provided by VSU) and electronics enabled us to obtain spectra free of background out to 15 microseconds (figure 2 shows a MuSR spectrum taken on aluminum).

There were two runs at Brookhaven in 1984, mid-March to early April and mid-May to mid-June. The March/April run was devoted primarily to beam development. During the May/June run several successful experiments were performed. The effect of uniaxial strain on an Fe(Si) crystal at elevated temperature (360K) was measured and the results were incorporated in the paper attached to this report as Appendix 1. This paper includes a complete analysis of Fe pulling data taken earlier at the Swiss Institute for Nuclear Research (SIN), which was supported in part by NASA grant NSG-1342. The paper has been submitted to Physical Review B.

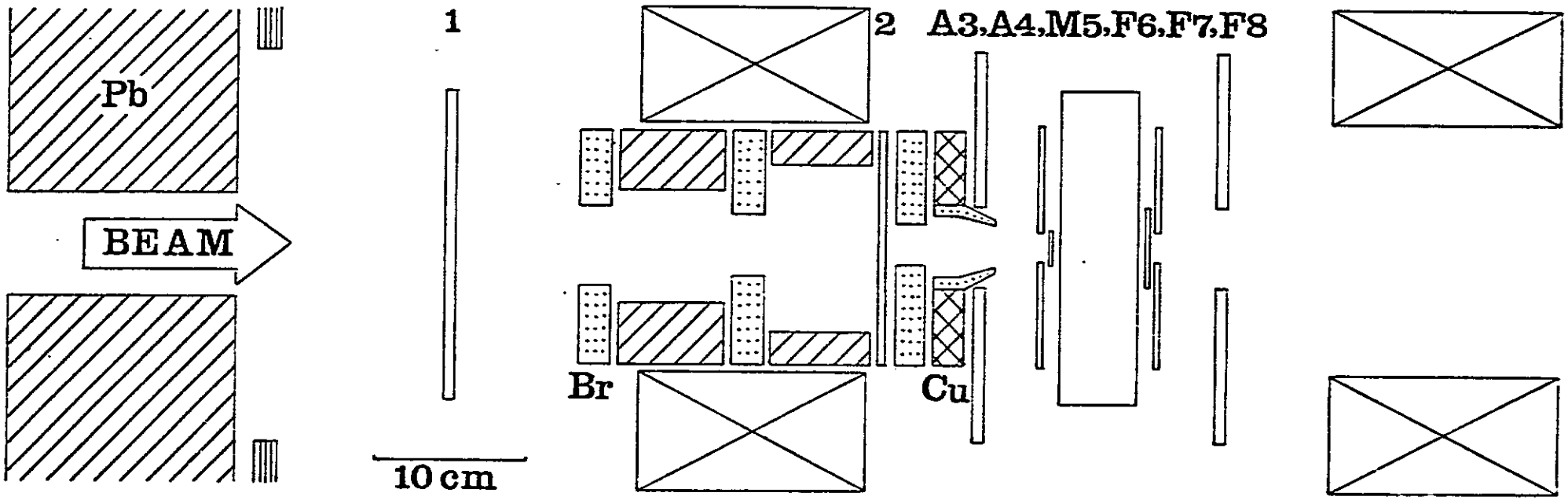

Figure 1. Muon collimation system at BNL.

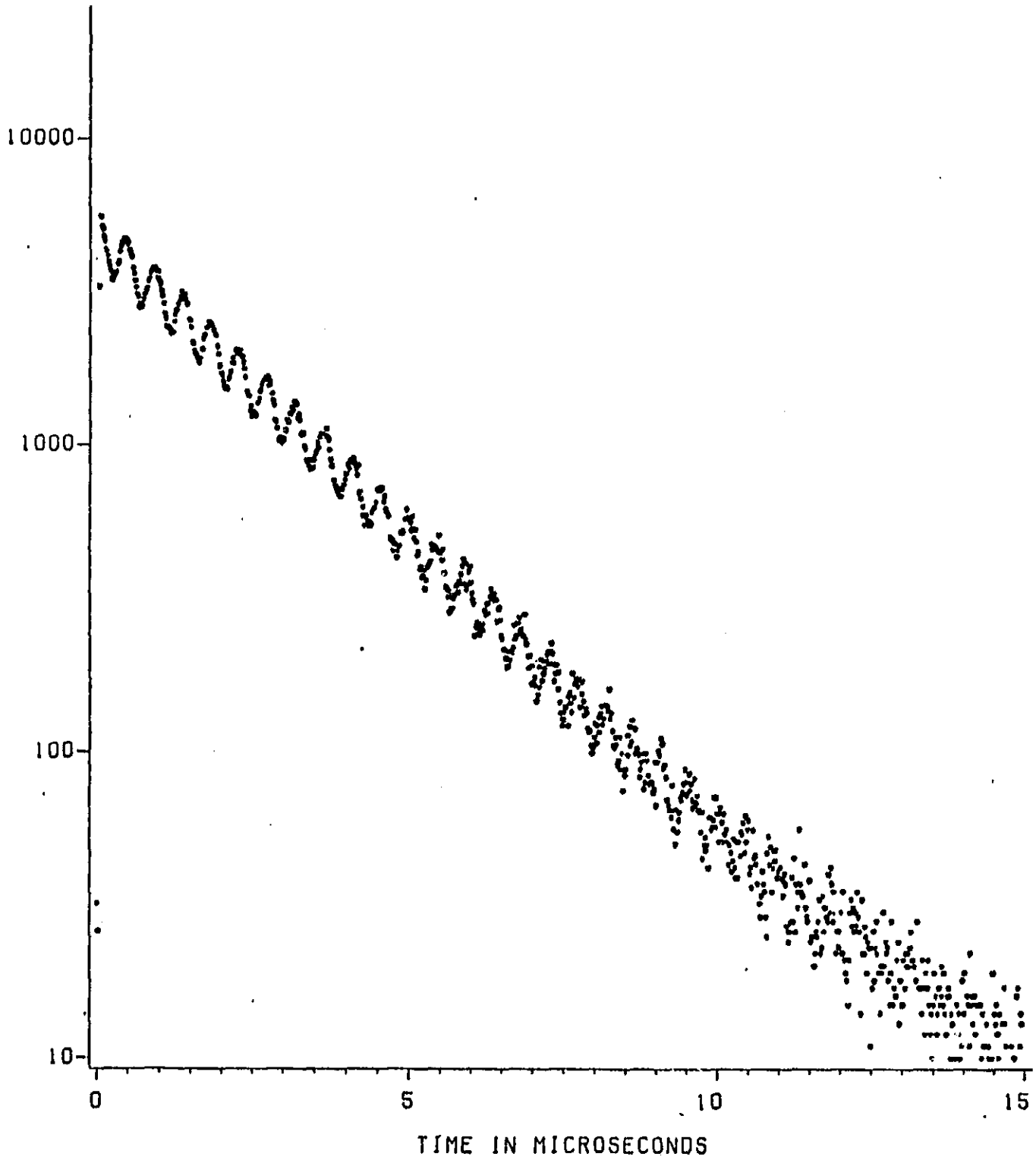

Figure 2. MuSRspectrum from Al.

Figure 3 shows the depolarization of positive muons as a function of temperature in titanium hydride. The dip at about 200K is an expected effect due to trapping/detrapping at impurity sites. There is no clearcut explanation for the dip beginning at about 280K, although we suspect it may arise from a shift of the muons from tetrahedral to mixed tetrahedral/octahedral sites in the crystal. Experiments were also done on niobium hydride. Papers on both of these experiments are in preparation and will be included in future progress reports. An abstract submitted to the March 1985 American Physical Society meeting is included as Appendix 2.

A set of iron alloys (mostly with transition elements) was also studied and an abstract was submitted to the same March 1985 APS meeting (to be held in Baltimore) is included as Appendix 3.

Further analysis was done on the MuSR data on nickel alloys studied at SIN in August/September 1983, and supported in part by NASA grant NSG 1342. An abstract of a talk presented at the January 1985 American Physical Society meeting (held in Toronto) plus a table of fractional changes in muon field, Lorentz field and hyperfine field with impurity concentration are included as Appendix 4. The director also gave a talk on these studies at the Virginia Academy of Science meeting held in May 1984 in Richmond.

The VSU participants in these experiments were Carey E. Stronach, director of the institute, and Lucian R. Goode, Jr., a physics graduate student. Michael Davis, an undergraduate, participated in preliminary preparations at VSU. The Brookhaven program is under the overall leadership of William J. Kossler, professor of physics at the College of William and Mary. Other participants included William F. Lankford of George Mason University, Harlan Schone of William and Mary, Anthony T. Fiory of Bell Labs, Robert I. Grynszpan of CNRS,

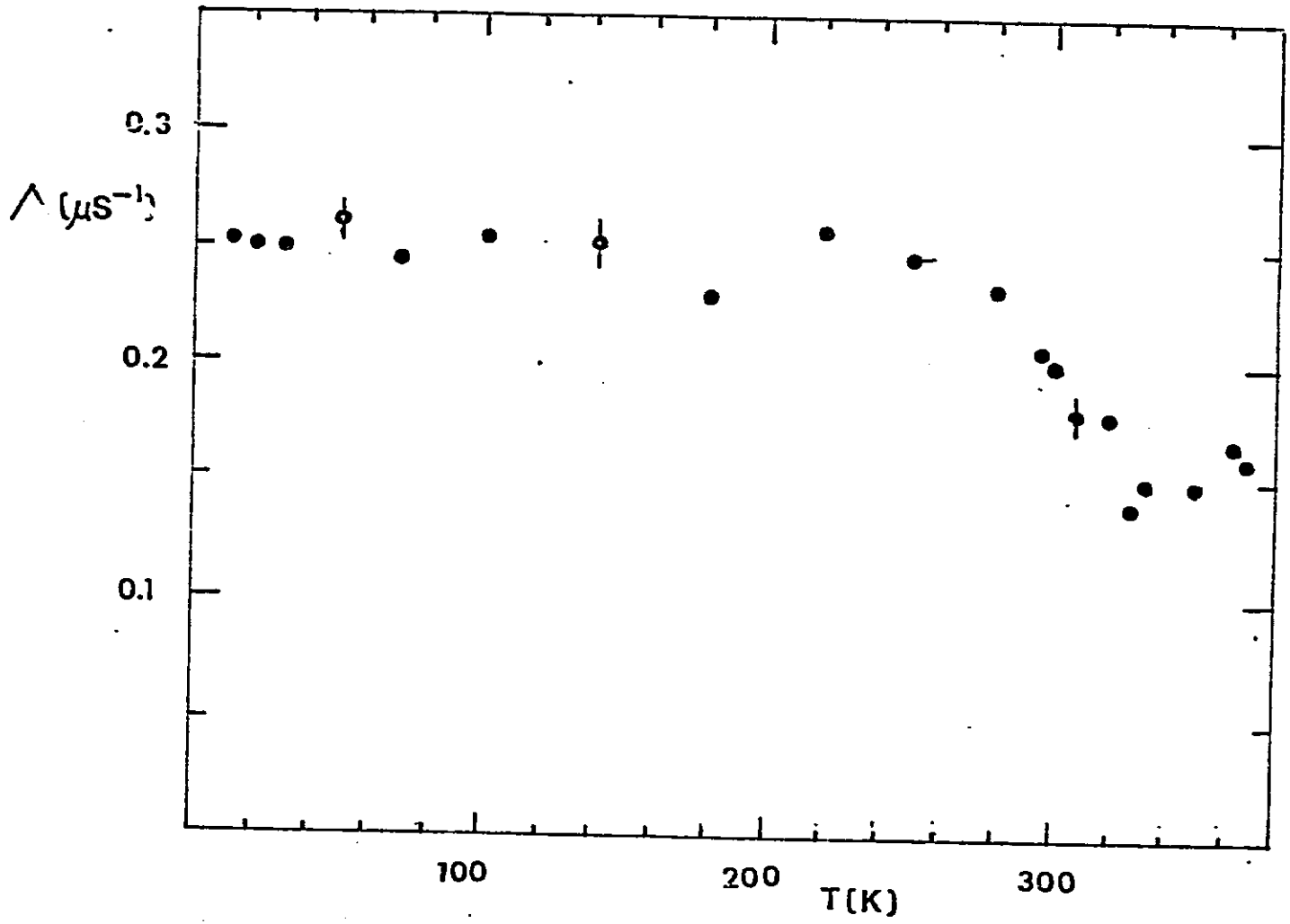

Figure 3. MuSR depolarization rate in titanium hydride as a function of temperature.

Vitry, France, and three graduate students from the College of William and Mary. The titanium hydride experiments also included Ola Hartmann and Roger Wäppling of the University of Uppsala in Sweden.

Additional experiments are being planned for the Brookhaven facility, and are currently scheduled for several running segments between February and June 1985. These are expected to include further studies of iron alloys, measurement of frequency shifts in strained single crystals of nickel, and measurement of depolarization in GaAs.

Hall Effect Studies

The overall objectives for the year were accomplished. The literature was analyzed and some of the equipment was ordered and received. Contacts were established with the Francis Bitter National Magnet Laboratory at the Massachusetts Institute of Technology. Undergraduate and graduate students were involved in the effort.

An analysis of the literature led to the conclusion that Hall effect studies of proton-damaged semiconductors can provide new information on the nature of defects and dislocations in gallium arsenide. The literature does not report any significant Hall studies performed on radiation damaged semiconductors. It appears that we are in virgin territory. Plans were made accordingly for experiments at the Naval Research Laboratory in 1985.

The involvement of students in the project has been significant, in particular on the undergraduate level. Five undergraduate students are developing

experimental techniques as well as basic knowledge of thin film deposition, data acquisition, and, most importantly, Hall effect measurements.

The addition of a magnet power supply and gaussmeter has brought the Hall effect measuring system to the capability of measuring Hall voltages at room temperature. We anticipate adding a data acquisition system and a cryogenic system to it in 1985.

The goals for 1985 have been established. First plans are to formulate a theoretical basis for relating galvanometric measurements (Hall effect and magnetoresistance) to defects in solids. Second, to perform a series of experiments leading to results which will establish relationships between variations in Hall voltage and the type and density of defects in the semiconductor samples.

Computer Simulation of Radiation Damage in Semiconductors

The main objective of this research project,"Computer Simulation of Defects Produced in Proton and Electron Irradiated Gallium Arsenide", is to develop a computer code to simulate the defect formation in proton and electron irradiated gallium arsenide and the diffusing of these defects within the crystalline structure. The primary focus of the first phase of this research project was to develop a computer code that could be used to simulate radiation damage in semiconductors. The diffusion aspects of the problem will be approached during the final stages of the project. This report describes progress which has been made to date on this phase of the research.

A search of the literature yielded a description of the binary-collision simulation code MARLOWE, which appeared to be applicable to this particular problem. The original code was written by Mark T. Robinson of ORNL and Ian M. Torrens of The Center for Nuclear Studies in Saclay, France. A copy of this code was purchased from the National Software Center which is located at Argonne National Laboratory. This code was then studied and analyzed. Subsequently, it was modified for use on NASA Langley Research Center's computer system. Due to the extra large amount of memory required by the code during simulation, it could only be run on the Cyber 205. The tasks of modifying and debugging the code required approximately eleven months. The modified code has been renamed and is now on file in NASA LRC's system under the name of MARS.

MARS can be used for the simulation of atomic displacement cascades in a variety of crystalline solids, using the

binary-collision approximation to construct the projectiles' trajectories. The atomic scattering is governed by the Moliére potential. Impact-parameter-dependent inelastic losses are included which involve a modified-Firsov electronic stopping model. Thermal vibrations of the target atoms and crystal surfaces may be included. Permanent displacement of the lattice atoms may be based on either an energy-threshold criterion or a Frenkel-separation criterion.

The computer program starts with a primary recoil atom of specified energy, position, and direction. This projectile is followed through a series of inelastic binary atomic collisions. If the energies which they receive are sufficiently great, the target atoms in these collisions will be added to the cascade. To simulate the development of the cascade in time, the program always follows the current fastest particle. When the energy of a particle becomes sufficiently small, or it escapes from the target material, or meets certain preassigned conditions, it is dropped from the cascade. If no particles remain to be followed, various analyses of the results of the calculations are performed.

A theorectical understanding of displacement effects in semiconductors requires a detailed analysis of the dependence of the number of point defects produced and their spatial distribution on the energies of the primary recoil atoms. These atoms, originally set into motion by interactions with incident electrons, protons, neutrons, or ions dissipate their initial kinetic energies in a series of inelastic encounters with other

atoms of the semiconductor, displacing some of these atoms,which then slow down by a similar series of collisions. The resulting cascade of displaced atoms and their accompanying vacancies are eventually responsible for the changes which occur in the irradiated semiconductor. These may include erosion of the target, alteration in its physical properties or chemical composition.

MARS, a modified version of the binary-collision simulation code MARLOWE, was used to simulate atomic displacement cascades in the semiconductor gallium arsenide. This semiconductor was chosen because of the wide range of interest in this material for the construction of solid state devices which may be used in an environment where exposure to radiation is highly probable.

The model used in the simulation of radiation damage in gallium arsenide was set up using the parameters described in the following statements. The threshold displacement energies were taken to be 8.8 and 10.1 ev. for gallium and arsenic atoms, respectively. Projectile cutoff energy was taken for all projectiles as 4.0 ev. The maximum impact parameter was .62 times the lattice constant and a screening length of 0.0738 was used in the Moliere potential. Inelastic losses, both local and nonlocal, were included. Thermal displacements were not included . The directions of the primary recoil atoms were selected statistically using Monte Carlo technique. Permanent displacement of lattice atoms was based on the Frenkel-pair criterion.

Some preliminary results for the simulation of radiation damage in gallium arsenide are presented on the included graphs.

These results were obtained using primary recoil atoms having energies of 20,40,60,80, and 100ev. One hundred cascades of primary recoil atoms were generated for each energy. The plots represent the average number of occurrences per cascade.

We are now in the process of interpreting the results gathered from the simulation in order to make refinements in the model that is to be used in future simulations.

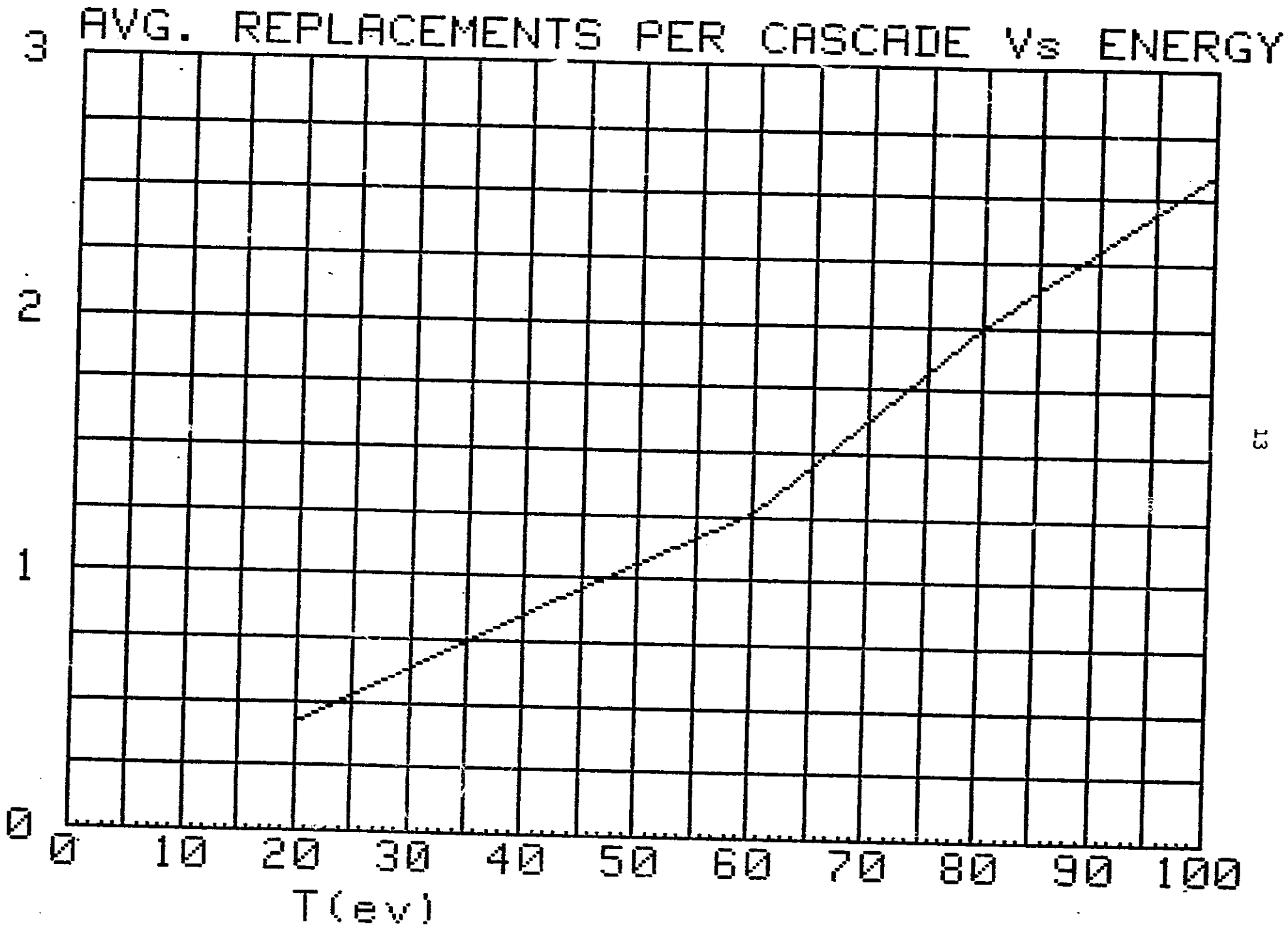
AVG. REPLACEMENTS PER CASCADE Vs ENERGY
3
2
1
0
0
10
20
30
40
50
60
70
80
90
100
T(ev)

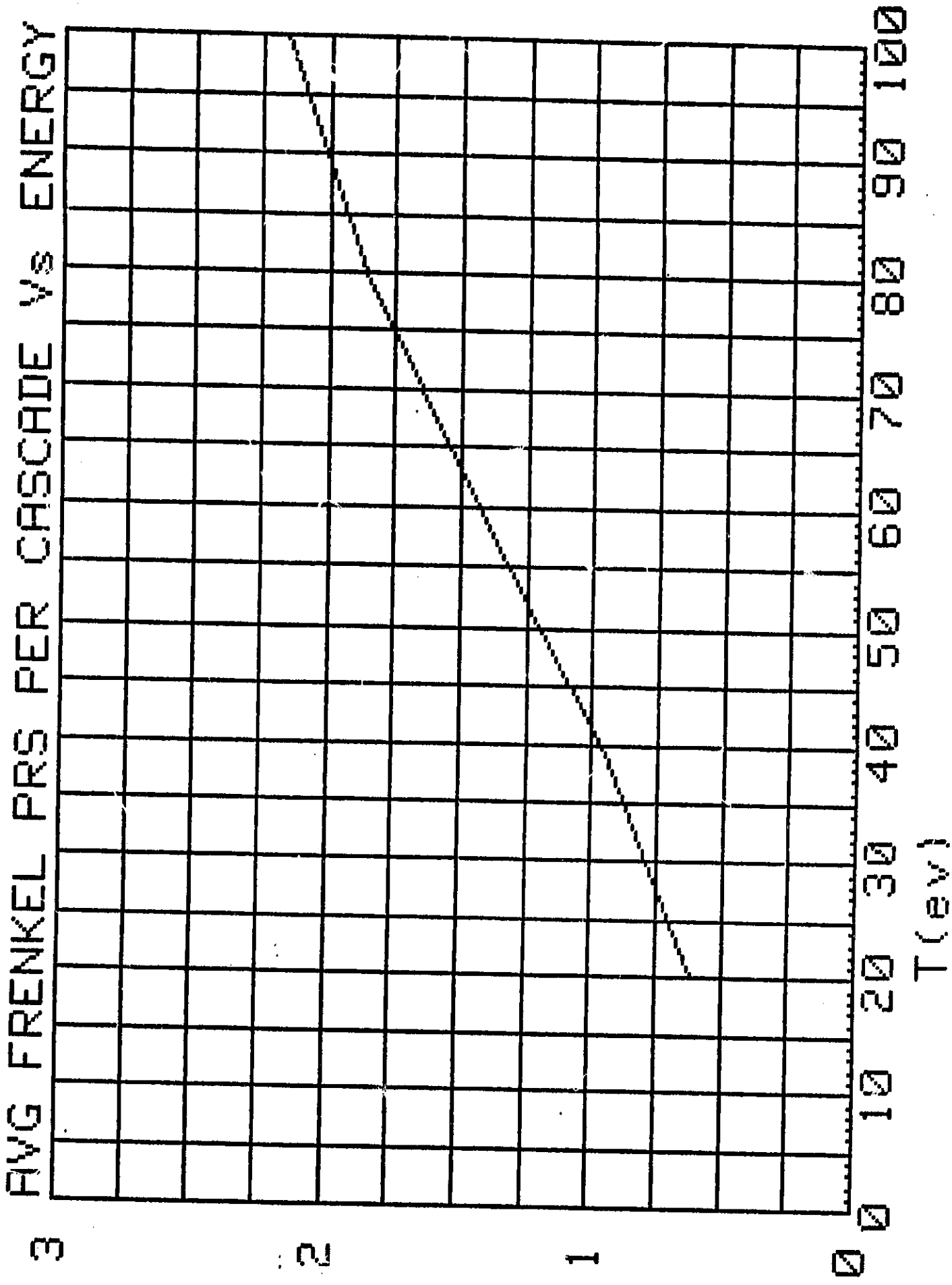
AVG FRENKEL PRS PER CASCADE Vs ENERGY
3
2
1
0
0 10 20 30 40 50 60 70 80 90 100
T(ev)

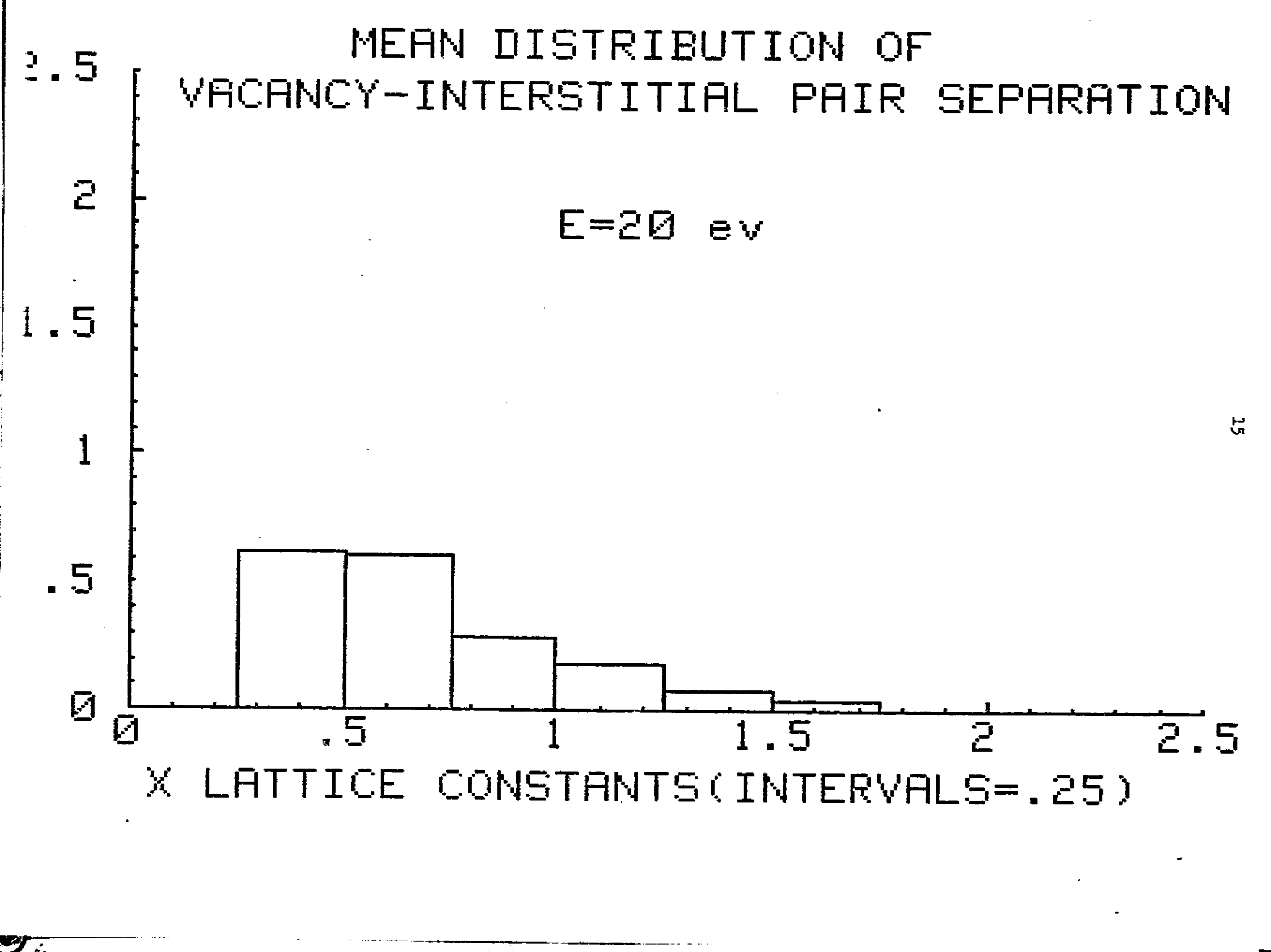
MEAN DISTRIBUTION OF
VACANCY-INTERSTITIAL PAIR SEPARATION
E=20 ev
2.5
2
1.5
1
.5
0
0
.5
1
1.5
2
2.5
X LATTICE CONSTANTS(INTERVALS=.25)

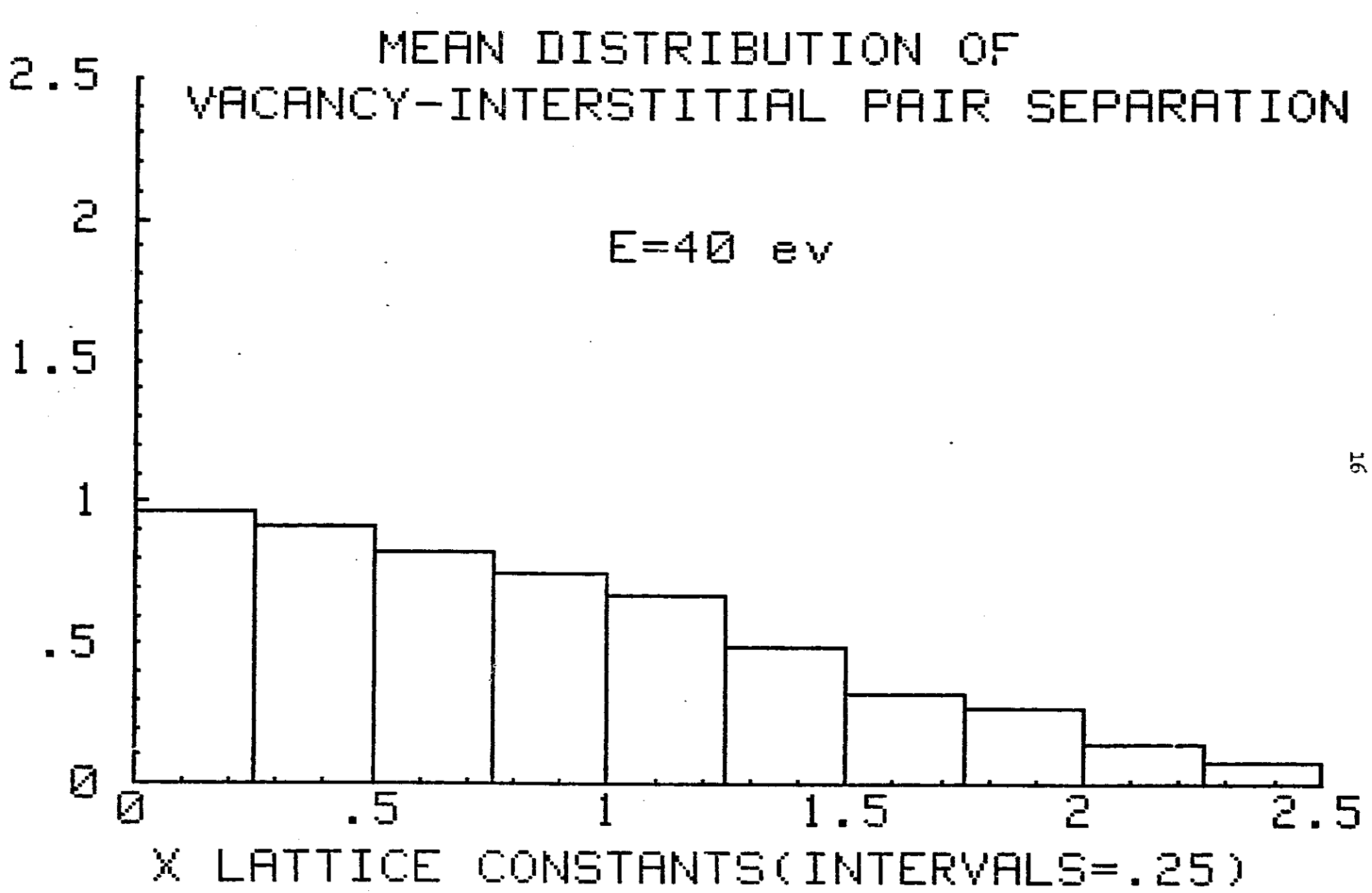
MEAN DISTRIBUTION OF
VACANCY-INTERSTITIAL PAIR SEPARATION
E=40 ev
2.5
2
1.5
1
.5
0
0
.5
1
1.5
2
2.5
X LATTICE CONSTANTS(INTERVALS=.25)

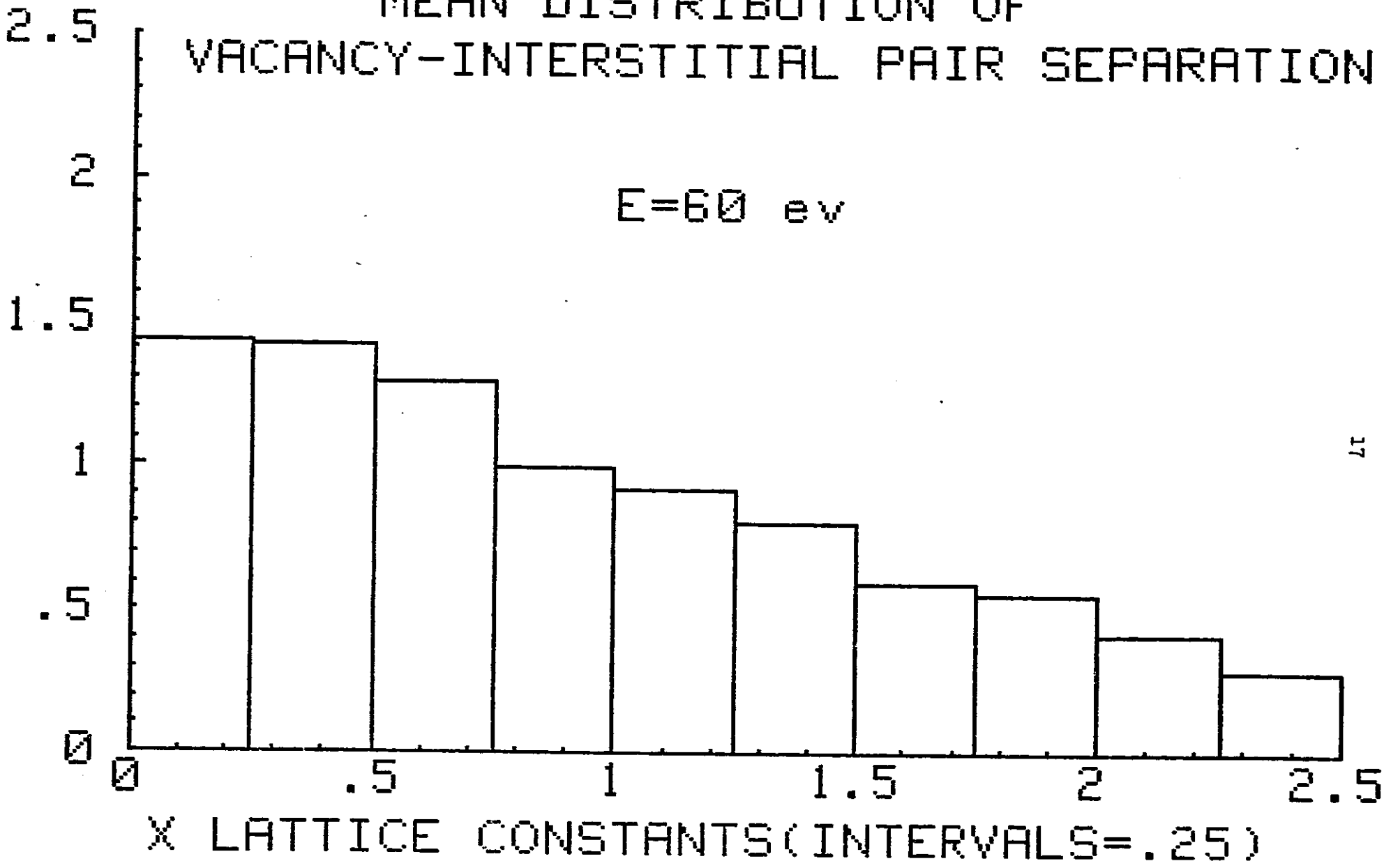
MEAN DISTRIBUTION OF
VACANCY-INTERSTITIAL PAIR SEPARATION
E=60 ev
2.5
2
1.5
1
.5
0
0
.5
1
1.5
2
2.5
X LATTICE CONSTANTS(INTERVALS=.25)

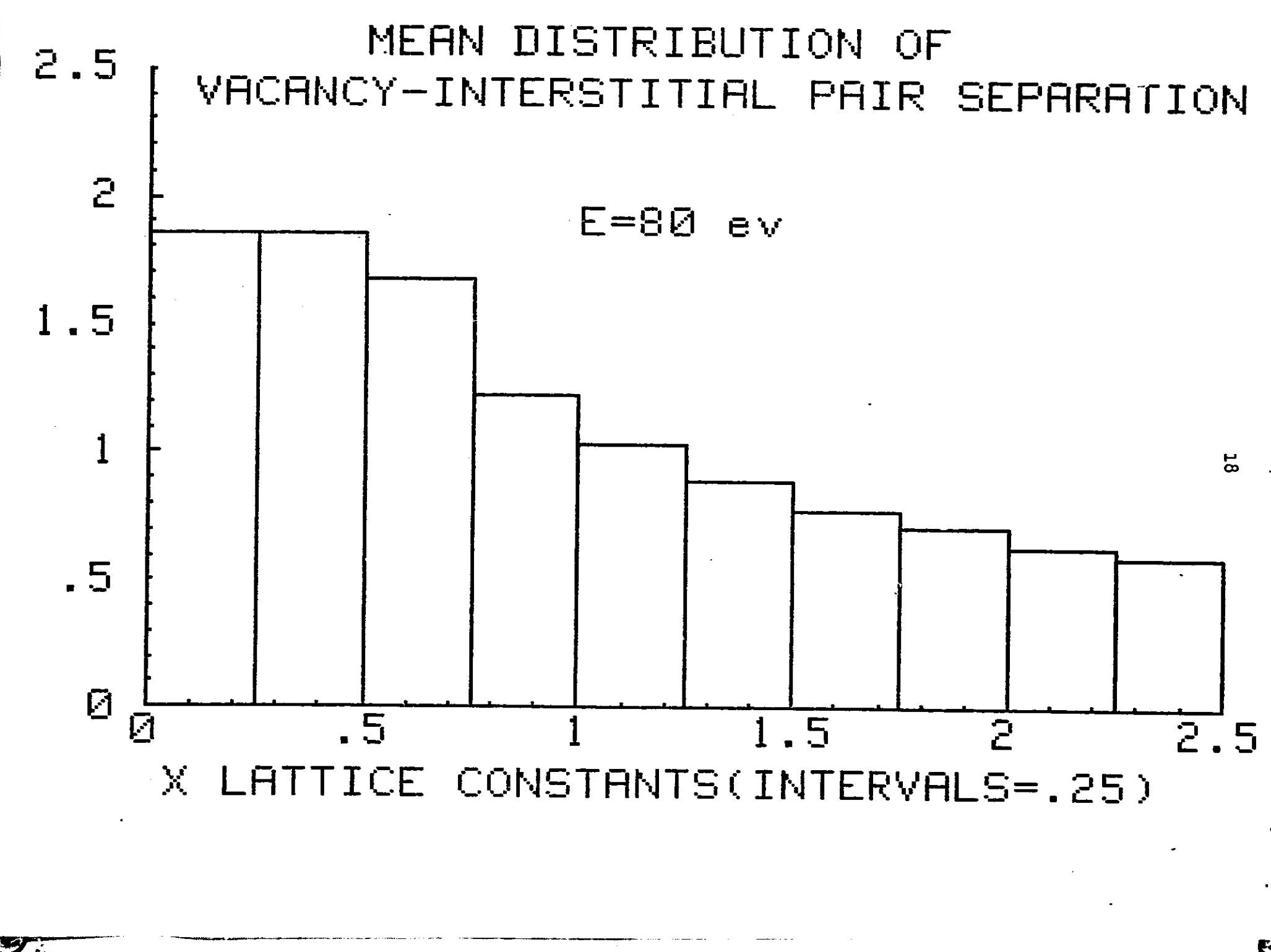
MEAN DISTRIBUTION OF
VACANCY-INTERSTITIAL PAIR SEPARATION
E=80 ev
2.5
2
1.5
1
.5
0
0
.5
1
1.5
2
2.5
X LATTICE CONSTANTS(INTERVALS=.25)

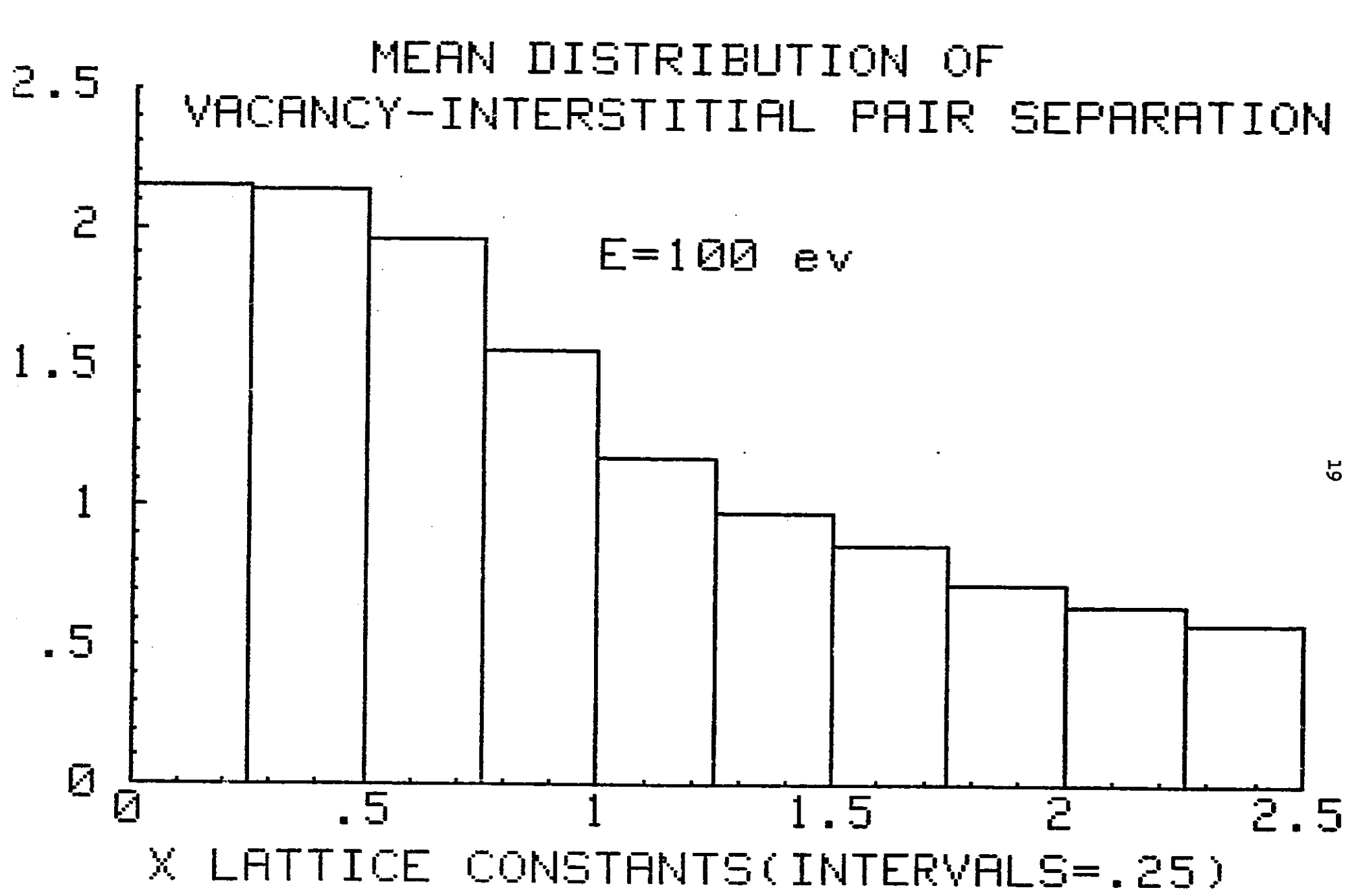
MEAN DISTRIBUTION OF
VACANCY-INTERSTITIAL PAIR SEPARATION
E=100 ev
2.5
2
1.5
1
.5
0
0
.5
1
1.5
2
2.5
X LATTICE CONSTANTS(INTERVALS=.25)

Student Participation

During the Spring 1984 semester two graduate students were working on thesis projects, Lucian R. Goode, Jr., and Akpan E. Akpan. Goode is working on muon spin rotation in iron alloys and Akpan on computer modeling of radiation damage in solids. Both should complete their M.S. degrees in the spring of 1985. Two other graduate students also participated, Deborah Brooks and Festus Onasoga. Brooks is seeking an M.S. in geophysics and Onasoga is seeking an M.S. in industrial arts (electronics).

In September 1984 three additional graduate students joined the program, Nana Adu, William Bolden and Larry Brown. Adu is working on muon spin rotation, while Bolden and Brown are working on radiation damage in solids.

During the Spring 1984 semester the undergraduate participants were Michael Davis, Candice Poarch Baines and Roscoe Ledbetter. During the Fall 1984 semester the undergraduate participants were Davis, Ledbetter, Cornelia Belsches and Raymond Noel.

Other Activities

The director of the institute participated in two experiments at the Los Alamos Meson Physics Facility in New Mexico during July/August of 1984. These were a study of gamma rays observed in coincidence with pionic X rays following negative pion absorption on ^{12}C, and a measurement of the distribution of inelastically scattered protons in coincidence with the 15.1-MeV gamma ray from an excited state of ^{12}C. Keshav N. Srivastava, associate professor of physics at VSU, also participated in the former experiment. Other collaborators included

Bernard J. Lieb of George Mason University, Herbert O. Funsten of the College of William and Mary, Hans S. Plendl of Florida State University, V. Gordon Lind of Utah State University, James Reidy of the University of Mississippi, and one graduate student each from Florida State and Utah State.

Even though these experiments were not part of the original proposal their intrinsic interest was of such high quality that we decided to participate, especially in light of the fact that the other collaborators felt the VSU participation was vital to the success of the experiments. The experiments were successful and we hope to continue this involvement. We doplan to find other sources of funding for this program in the future, and have submitted a proposal to the Department of Energy.

The director participated in the completion of a paper based on pion-nucleus experiments supported in part by NASA grant NSG 1646 in 1980. This paper has been submitted to Physical Review C and is attached to this report as Appendix 5.

The director of the institute was elected to the Board of Trustees of the Southeastern Universities Research Association (SURA) in October 1983. SURA plans to construct a 4-GeV electron accelerator in Newport News, VA, pending approval of funding by Congress. It is also planning research programs involving supercomputers, material science, and astronomy.

In May 1984 the director was also elected chairman of the astronomy, mathematics and physics section of the Virginia Academy of Science for the 1984-85 year. These two activities should complement his work as director because of their close relationship to physics research.

James C. Davenport served as director of the summer student program at

Fermilab (Batavia, Illinois) during the summer of 1984. He also served on the Committee on Minorities in Physics of the American Physical Society this past year. John J. Stith served as a summer research fellow at the NASA Langley Research Center during the summer of 1984.

Equipment and Supplies

The following items were purchased during the reporting period:

Muon collimation apparatus
3 EMI 9907B phototubes
3 Ortec 265 tube bases
6 Ortec 218 Mu metal shields
4 PVC inserts for phototubes
4 Fe shields for phototubes
Mo, Ge, Pt, As, Ta and W samples for Hall effect studies
1 digital multimeter
1 pocket multimeter
1 standard cell
set of batteries
assorted tools
diffusion pump oil
O rings
replacement of crystal in Ge(Li) detector
repair of Keithley 181 nanovoltmeter
100 reprints of a paper on pion reactions
50V-50A power supply for magnet plus accessories
Hall effect gaussmeter
Unibus cable

In addition, an internal account was set up at Brookhaven National Laboratory. This enables the institute to purchase equipment, supplies and materials from BNL directly while experiments are in progress.

A PDP 11/73 computer with 1 MB RAM, floppy disks, a 31-MB Winchester hard disk, and a color graphics terminal has been ordered. We plan to order additional peripherals (printer, plotter, modem, IEEE bus) with funds from the 1985 budget.

A Janis "Supertran" helium transfer tube is also on order. It will be

used as part of the cryogenics systems in MuSR and Hall effect experiments.

Summary

The initial year of this support from NASA has been most successful. We anticipate that the groundwork laid during 1984 will lead to substantial accomplishments during 1985: publication of additional MuSR papers, major results in the radiation damage studies, full operation of the Hall effect program, extensive student participation, completion of two Master of Science theses, and the installation of a high-quality scientific computing system.

The funding of the joint United States/France research program in muon spin rotation and the possible expansion of the MuSR facilities at Brookhaven National Laboratory make for a most favorable prognosis in that area.

We appreciate the support we are receiving from NASA and plan to continue making efficient and effective use of the funding.

Respectfully submitted,

Carey E. Stronach

Carey E. Stronach

Director

February 12, 1985

Uniaxial stress induced symmetry breaking for muon sites in Fe

W. J. Kossler, M. Namkung*, B. Hitti, Y. Li, and J. Kempton
Physics Department
College of William and Mary
Williamsburg, VA 23185 USA

C. E. Stronach, and L. R. Goode, Jr.
Physics Department
Virginia State University
Petersburg, VA 23803 USA

W. F. Lankford
Physics Department
George Mason University
Fairfax, VA 22030 USA

B. D. Patterson and W. Kündig
Physik-Institut der Universität Zürich
CH-8001 Zürich, SWITZERLAND

R. I. Grynszpan
CNRS, CECM
94400 Vitry, FRANCE

*Current address: NASA Langley Research Center, Hampton, VA 23665

Abstract

Uniaxial stress has been used on Fe single crystals to induce muon precession frequency shifts. The frequency shift for a nominally pure Fe sample at 302K was $-0.34 \pm .023$ MHz per 100 micro-strain along the <100> magnetization axis. This corresponds to a change of magnetic field at the muon of 25.1 ± 1.6G/100με. For an Fe (3wt%Si) single crystal the shifts were $-0.348 \pm .008$ MHz/100με ($25.7 \pm .5$G/100με at 300K), and $-0.279 \pm .010$ MHz/100με ($20.6 \pm .7$G/100με at 360K). The agreement between the shifts for Fe and Fe(3wt%Si) shows the effect to be intrinsic to iron and not strongly impurity sensitive. These shifts and their temperature dependence (1/T) are dominated by the effect of strain-induced population shifts between crystallographically equivalent, but magnetically inequivalent sites. Their magnitudes are in good agreement with theoretical predictions by Jena, Manninen, Niemenin, and Puska and by extrapolation from calculations on Nb and V by Sugimoto and Fukai, especially if both 4T(0) and 1T sites contribute comparably.

I. Introduction

The positive muon, having a rest mass of 105 MeV, may be viewed as a light isotope of hydrogen, the electronically simplest charged impurity, which can be added to metals. There are a number of questions of fundamental interest related to μ^+ implanted in metals; these include: where does the muon reside, how does it interact with lattice atoms, and how does its presence disturb the local electronic structure in ferromagnetic crystals?

In this paper we present a study of the muon's interaction with the lattice in which uniaxial stress induces an energy difference between crystallographically equivalent but magnetically inequivalent sites in an Fe single crystal.

Of the parameters measured, the precession frequency of the muon, which is proportional to the average local magnetic field is of particular interest. This local field is decomposed as:

$$\vec{B}_\mu = \vec{B}_{ext} + \vec{B}_{dem} + \vec{B}_L + \langle \vec{B}_d \rangle + \vec{B}_{HF} \qquad (1)$$

where $\vec{B}_{ext}$ is the applied external field, $\vec{B}_{dem}$ is the demagnetization field due to the finite and particular shape of the sample, and $\vec{B}_L$ is the Lorentz field which appears inside a spherical cavity within the sample. $\langle \vec{B}_d \rangle$ arises from the magnetic dipoles inside the Lorentz cavity appropriately thermally averaged over magnetically inequivalent sites, but not from the contact hyperfine interaction which is included as $\vec{B}_{HF}$. The site correlation time is probably less than 10^{-11}s at room temperature. For a general review of the

experimental and theoretical situation for muons in ferromagnetic material see, e.g.: Meier et al.[1] or Kanamori et al.[2].

We are interested in the change of $\vec{B}_\mu$ with applied uniaxial stress: $\Delta\vec{B}_\mu$. Changes in $\vec{B}_{ext}$, $\vec{B}_{dem}$ and $\vec{B}_L$ will be shown to be small for our purposes. Two features of the hyperfine field can be considered: the change with distance, especially with respect to the nearest neighbors; and differences in hyperfine field from one magnetically inequivalent, but crystallographically equivalent site to another. The first can be estimated from the measurements of Butz et al.[3] for Fe under homogeneous compression. As will be seen, in the Results and Discussion section this is a small effect and will (essentially) be ignored. The second is not usually calculated since there is no clear mechanism to introduce such a difference, further this difference would be multiplied by a small factor and so is ignorable unless it is of the order of the hyperfine field itself.

The remaining terms are primarily from the displacement of the nearest neighbor dipoles and from the changes in the thermal average, both induced by strain. By far the larger of these two is the strain-induced symmetry-breaking change in the thermal average, which may be written as:

$$\Delta B_\mu = 2/9(B_\ell - B_t)\Delta E/kT$$

where $\Delta E = -\left(\frac{S_{11}-S_{12}}{S_{11}}\right)(P_1-P_2)\varepsilon_{100}$, S_{ij} are the elastic compliances for Fe, P_i are the diagonal elements of the double force tensor[4] associated with the muon in Fe, $(B_\ell-B_t)$ is the difference in magnetic fields for the magnetically inequivalent sites, and ε_{100} is the strain along the <100> direction, which is also the magnetization axis. $(B_\ell-B_t)$ is essentially 3/2 B_ℓ, which in

turn depends strongly on lattice site, local lattice distortion, and the shape of the muon's wave function while executing its zero point motion. The double force tensor depends on the lattice site and the muon-Fe interaction, which then determines the lattice distortion and muon wave function.

Sugimoto and Fukai[5] have considered the behavior of protons and muons in the bcc metals obtaining P_1-P_2 for Nb and V.[5] We use their results below to extrapolate to Fe. We also compare to the results of Jena et al.[6], who calculate the shifts one measures using the effective medium model.

Yagi et al.[7] use the temperature dependence of the relaxation rates Γ_2^{100} and Γ_1^{111} to suggest a different intrinsic muon motion below 40K, and possibly preferential occupancy of the T sites (i.e. Fig. 1) at the lower temperatures and of O and T at higher temperatures. The dependence on angle between $\vec{B}_{app}$ and <100> of Γ indicates a site with tetragonal symmetry i.e. T or O or a linear combination. Hydrogen in bcc lattices typically seems to have T occupancy. Larger impurities in Fe force a lattice relaxation which is large enough to favor the O site.[8] The calculations of Sugimoto and Fukai suggest that the larger zero point motion of the muon causes it to behave as though it were larger than the proton and hence favor the 4T(O) site.[5]

A perplexing feature of μSR with Fe alloyed with small quantities of other elements or Fe with high dislocation density has been the general tendency for the magnetic field at the muon to decrease in magnitude once one has taken the magnetization changes into account.[9] The present study leads to the suggestion that internal strains are responsible for the effect.

II. Experiment

A. Beam Lines, μSR and Pulling Apparatus

These measurements were done at the Swiss Institute for Nuclear Research (SIN) for a pure Fe single crystal, and at the AGS of Brookhaven National Laboratory (BNL) for a Fe (3wt%Si) single crystal.

At BNL we used beam line D2, the decay channel for stopping muons, which we with A. Sachs, J. Fox and R. Cohen designed and had installed. The μSR apparatus there is shown in Fig. 2. For 10^{12} protons per AGS cycle on the production target we had 6000 muons through the last collimator (2.3 cm diameter) and detector M5, 1800 stops in the sample, and 350 events. Six trim coils were used to cancel residual magnetic fields and field gradients at the sample. A large Helmholtz pair, indicated in the figure produced the aligning field. Typical asymmetries were 14%, somewhat lower than the 18% observed for non-magnetic material. 18% corresponds in our detector geometry to about 80% polarization in the beam.

At SIN a surface beam from the π E3 port was sent through a 2 x 3 mm collimator of the MiLi μSR apparatus. A positron event rate of 2000 was achieved for detectors forward and backward with respect to the beam from the sample position. A jig was used to mount the sample in order to prevent misalignment between the stress direction and the long axis of the samples. A support for the sample was used during the mounting and dismounting process to minimize extraneous mechanical strains.

Figure 3 shows the arrangement of the puller. The sample was typically held in position with epoxy. Since the epoxy was found to soften at 360 K, grooves were cut in the Fe(3wt%Si) sample which mated to ridges in the holder.

The sample holder assembly was insulated by a vacuum jacket. For the pure Fe sample, 302K was maintained by circulating ethanol at a carefully controlled temperature through the cooling line. For all samples temperature was monitored with a Pt resistor. The 300 K temperature was measured to be nearly constant, without control throughout the data taking at BNL. For 360 K temperature, monitored and controlled water was circulated through the tubes. A temperature difference occurred at the sample for the maximum stress on, and subsequent stress released, 360 K point, arising from reduced thermal contact with the Pt resistor associated with melting of the conductive grease. This error was estimated to be 3 K and has been corrected for in plotting the data.

B. Samples

For these experiments we used two single crystal samples. The first (Fe) was nominally pure iron while the second was iron alloyed with 3 wt% Si. Both samples were supplied by Monocrystals Co. of Cleveland, Ohio.

The Fe single crystal was prepared from a polycrystalline Armco iron ingot which was grown by the strain-anneal method. The sample then was cut using thin abrasive saws and point mills. A chemical etch was used to clean the surfaces and remove surface damage. Final dimensions were $1 \times 4.6 \times 46.13\ mm^3$, with the <100> along the long axis and the <010> 10° from

the flat surface normal. Neutron activation analysis indicates 800 ppm Cu and 500 ppm Mn to be the primary heavy impurities in this sample. The concentrations of C and O were not determined.

The Fe (3wt%Si) crystal was grown in vacuum by the Bridgman method from alloy stock which was prepared by intermixing powdered iron (electrolytic grade, 99.52% Fe, .04% H, .04% C and .05% other) with silicon powder from the Union Carbide Electromet Division. A <100> axis was determined by X-rays and the sample cut and treated by the same techniques used for the pure Fe crystal. Final dimensions were: 2.8 x 10 x 50 mm^3, the long axis being <100> and the <010> axis 14° from the wide-surface perpendicular. To facilitate pulling, especially at elevated temperatures, grooves 2 mm wide and 1 mm deep were cut in the wide surfaces 2 mm from the ends of the sample using an electro-discharge milling machine.

C. Strain Measurements

Strain was induced in the sample by uniaxial stress along the <100> direction applied by a piston and compressed air arrangement for the pure Fe experiment and by dead weights for the Fe(3wt%Si) sample. At 300 K the strain was directly measured using a strain gauge. For 360 K the strain was inferred from the stress and elastic constant, which later was obtained by reducing our 300 K constant by the ratio of elastic constants at 360 K and 300 K of reference 10. Table I shows our values of strain.

Table I

Weight kg	ε_{xx} (μ-strain) 300 K	360 K
29.5	82.4	78.6
59.2	169.6	161.9

D. Data Analysis

We used the model functions:

$$N_{F,B}(t) = N_{0_{F,B}} e^{-t/\tau_\mu} [1 \pm p[F_\ell e^{-t/T_1} + F_t e^{-t/T_2} \cos(\omega_\mu t + \phi)]] + B_{F,B}$$

which include the effects of longitudinal as well as transverse domain polarization. $p = A \cdot P(t=0)$ where A is the effective asymmetry associated with the forward or backward detectors and energy spectrum of the positrons which are detected, and $P(t=0)$ is the muon polarization just after stopping in the sample. The parameters F_t and F_ℓ refer to the fraction of domains which are magnetized transversely and longitudinally, i.e. parallel, to the initial muon polarization.

In the actual fitting process F_ℓ was factored out of the bracket and F_t replaced by $\beta = F_t/F_\ell$ which corresponds to the ratio of volumes of domains perpendicular and parallel to the initial muon spin orientation. The forward and backward histograms of each run were analyzed simultaneously using one value for each parameter which, in principle, would be the same in both histograms.

In cases for which T_2 was short, e.g. with cold worked Fe, replacing e^{-t/T_2} by $e^{-\sigma^2 t^2}$ significantly reduced χ^2.

E. Domain Alignment with Field

For the pure iron sample, surface muons were used which stopped within about 0.1 mm of the surface of the sample. The sample had some surface irregularities and these in turn caused two problems: the domains near the surface were not naturally completely aligned along the long <100> axis; and there was a spatial inhomogeneity to the field.

Since the effect of stress is dependent on the orientation of the domain alignment with respect to the stress axis, several tests were made to verify that the working field was sufficient to bring the sample to essential saturation and domain alingment. Figure 4 indicates the μ precession frequency as a function of applied field. As one can see, the field penetrates above about 120 Oe for the pure iron sample and 350 Oe for the Fe(3wt%Si) sample. That the precession frequency drops as a function of external field is a reflection of the fact that the internal field is oppositely directed to that of the external field. A demagnetizing field of about these values are expected for ellipsoids of dimensions just inscribable in the rectangular samples. We also calculated the penetrating fields based on homogeneously magnetizeable rectangular samples. These are in rough agreement with the frequency fall-off.

A more direct measure of domain alignment is the ratio F_t/F_ℓ. While F_t includes domains not only along $\vec{B}_{ext}$, i.e., along the long axis of the sample, but also those transverse to that and the beam, i.e., longitudinal direction, it should be dominated by the domain fraction parallel to $\vec{B}_{ext}$. For perfect domain alignment F_t/F_ℓ goes to ∞. In Fig. 5 we can see for pure Fe that above $\vec{B}_{ext}$ = 120 G this ratio is very large and thus we can again conclude that there is essentially complete domain alignment. The F_t/F_ℓ ratios

obtained for our principal set of data on pure Fe, which was taken at 150 G, are plotted in Fig. 6. These show that the domain alignment remained high throughout.

For the Fe(3wt%Si) sample, for which we used the more uniformly stopping muons of the AGS decay beam, F_t/F_ℓ was always very high and independent of applied field. This clearly indicates that for this sample the domains were always predominantly aligned along the <100> axis parallel to the long axis of the sample, a result expected on energy grounds. For this sample we carried out the stress measurements at 325 Oe. At higher fields where the sample becomes completely magnetized the non-ellipsoidal shape produces some field inhomogeneities which are reflected in the depolarization rate increase seen in Fig. 6. Thus by staying at 325 Oe we were able to achieve better frequency accuracy.

III. Results

In Fig. 7 we show the observed precession frequencies for muons in pure Fe(a) at 302 K and in Fe(3wt%Si) at 300 K (b) and 360 K (c) as functions of strain along the <100> long axes of the samples. To check the reversibility we took stress-relieved data after each stress-applied point and these frequencies are shown along the horizontal lines. The best straight line fits to the measured points yield:

Table II

		Fe 302 K	Fe(3wt%Si) 300 K	Fe(3wt%Si) 360 K
$\frac{\partial \nu}{\partial \varepsilon}$	(MHz/100με)	-0.34 ± .023	-0.348 ± .007	-0.279 ± .010
$\frac{\partial B_\mu}{\partial \varepsilon}$	(G/100με)	25.1 ± 1.6	25.7 ± .5	20.6 ± .7

The hypothesis that the stress-relieved points correspond to a constant frequency is consistent with the data so that inelastic history-dependent effects do not seem to enter.

That the stress dependence of the frequency for pure Fe and Fe(3wt%Si) agree with each other at room temperature clearly indicates that these stress effects are intrinsic and not impurity sensitive.

The better frequency accuracy for the Fe(3wt%Si) sample reflects the slower depolarization rate (hence longer time base for that sample), perhaps a result of the more homogeneous fields deeper in the sample which could

be probed with the more penetrating decay beam and also the greater ease with which the alloy sample could be annealed to relieve internal strains at temperatures near melting. In contrast to pure Fe, the alloy here does not undergo the α-γ phase transition, when cooled from the melting point.

Interpretation of the Result for $\partial B_\mu/\partial\varepsilon$.

The derivative of $\vec{B}_\mu$, see eq. (1), with respect to strain is:

$$\frac{\partial \vec{B}_\mu}{\partial \varepsilon_{100}} = \frac{\partial \vec{B}_{ext}}{\partial \varepsilon_{100}} + \frac{\partial \vec{B}_{dem}}{\partial \varepsilon_{100}} + \frac{\partial \vec{B}_L}{\partial \varepsilon_{100}} + \frac{\partial \langle \vec{B}_d \rangle}{\partial \varepsilon_{100}} + \frac{\partial \vec{B}_{HF}}{\partial \varepsilon_{100}}$$

Clearly $\frac{\partial \vec{B}_{ext}}{\partial \varepsilon_{100}}$ is zero. The demagnetizing field is on the order of 125 Oe for pure Fe and 325 Oe for Fe(3wt%Si) and its fractional change with strain should be on the order of the strain, and thus for 100 με should only be about 1/100 of a Gauss and can be ignored.

$\vec{B}_L$, the cavity field, is $\frac{4\pi}{3}\vec{M}_s$, where $\vec{M}_s$ is the saturation magnetization. As far as we know, no direct measurement of $\frac{\partial M_s}{\partial \varepsilon}$ for a pure Fe crystal has been reported so we consider the following equation:[1]

$$\left(\frac{\partial \lambda_s}{\partial H}\right)_{\sigma,T} = \left(\frac{\partial M_s}{\partial \sigma}\right)_{H,T}$$

where λ_s is the saturation magnetostriction along the external field H. From the measurement of Calhoun et al.[12] $\left(\frac{\partial \lambda_s}{\partial H}\right)_{\sigma,T} = 2.3 \times 10^{-10}$/G along the <100> axis of a pure Fe crystal at room temperature. Therefore, we obtain $\left(\frac{\partial M_s}{\partial \sigma}\right)_{H,T} = 2.3 \times 10^{-4}$ G/bar which gives $\Delta M_s \cong .03$G for $\varepsilon_{100} = 100_{\mu\varepsilon}$. Hence the contribution of $\partial B_L/\partial \varepsilon_{100}$ will be neglected.

In the introduction we said that $\frac{\partial \vec{B}_{HF}}{\partial \varepsilon_{100}}$ is small. We now justify that statement in a little more detail.

The hyperfine field at the muon is usually written as:

$$B_{HF} = \frac{-8\pi}{3} \eta_{(o)} (\eta_o^+ - \eta_o^-) \mu_B$$

where $\eta_{(o)}$ represents the spin density enhancement produced by the positive charge of the muon and $(\eta_o^+ - \eta_o^-)$ is the intrinsic local spin density at the muon site. We ignore differences in hyperfine fields from one magnetically inequivalent site to another as there is no direct origin for such differences and they would in any case be multiplied by the strain, a small number. The changes in hyperfine field induced by uniaxial strain then must arise from the dependance on the radial distances from nearby Fe atoms. We use the homogeneous pressure results of Butz et al.[3] to make estimates for the derivative in two ways; first, by comparing local density changes, and second, by assuming the effect is dominated by nearest neighbors only.

According to Butz et al., $\Delta B_H \approx -3G$ for a positive volume strain of 300×10^{-6} in Fe. The corresponding value of $\Delta M_s = .234$ G can be obtained by combining the experimental results of $\frac{\partial \ell n M_s}{\partial p} = -.28 \times 10^{-3}$/kbar and $\partial \ell n V/\partial p = -.59 \times 10^{-3}$/kbar. Since the change in $(\eta_o^+ - \eta_o^-)$ follows roughly that of M_s, we estimate the change in B_{HF} by uniaxial stress to be -0.4 G for 100με.

Now assuming nn dominance we calculate for octahedral occupancy (the alternative tetrahedral occupancy would have a very small change with stress). Under uniaxial strain the average change in $\vec{B}_{HF}$ due to the two nn atoms, which are half a lattice constant, (a/2) away, is:

$$\left\langle \frac{\partial B_{HF}}{\partial \varepsilon_{100}} \right\rangle^{uni} = 2 \frac{\partial B_{HF}}{\partial Z} \frac{a}{2} - 4 \frac{\partial B_{HF}}{\partial Z} \frac{a}{2} \cdot \frac{1}{p}$$

The first term arises from sites with tetragonal axis parallel to the stress axis. $\rho = 2.74$ is the Poisson ratio for Fe corresponding to the transverse contraction associated with longitudinal elongation. For a strain of say $\varepsilon_{100} = 100\mu\varepsilon$ this leads to

$$\langle \Delta B_{HF} \rangle_u = a\,\varepsilon_{100}\,\frac{\partial B_{HF}}{\partial Z}\,(1-\frac{2}{\rho}).$$

The homogeneous pressure case yields

$$\langle \Delta B_{HF} \rangle_h = a\,\frac{\Delta V}{V}\,\frac{\partial B_{HF}}{\partial Z}$$

and, since a $300\,\mu\,\frac{\Delta V}{V}$ corresponds to a $100\,\mu$ strain, we have:

$$\langle \Delta B_{HF} \rangle_u = (1-\frac{2}{\rho})\,\frac{1}{3}\,\langle \Delta B_{HF} \rangle_h$$

This results in a $-.27$ G per 100 μ strain shift. This is even smaller than the first estimate and in both cases $\partial B_{HF}/\partial \varepsilon_{100}$ is small enough to be neglected.

Thus we are left with only $\partial \langle B_d \rangle / \partial \varepsilon_{100}$ as the dominant contribution for $\partial B_\mu / \partial \varepsilon_{100}$. The change in $\langle B_d \rangle$ by uniaxial stress arises from two effects. First, there is a change in the muon occupation probabilities between magnetically inequivalent sites where the signs and magnitudes of B_d are quite different; and second, uniaxial stress lowers the symmetry so that the sum of B_d over the three octa- or tetrahedral sites for an Fe unit cell is not zero anymore. We can combine these contributions to $\langle B_d \rangle$ as:

$$\langle B_d \rangle = +\frac{2}{9}\,(B_\ell - B_t)\,\frac{\Delta E}{kT} + \frac{1}{3}\,(B_\ell + 2B_t) \qquad (1)$$

where $\Delta E = -\frac{(S_{11} - S_{12})}{S_{11}} (P_1 - P_2)\varepsilon_{100}$ is the difference in free energies between the magnetically inequivalent sites, the S_{ij} are elastic constants, and P_i are diagonal elements of the double force tensor for the muon in Fe. For the case at hand, with strain along a <100> axis, the second term is negative and less than 5 G in magnitude for $\varepsilon_{100} = 100 \times 10^{-6}$ at either the octa- or tetrahedral sites. The sign of the first term, from our calculations, is positive and dominates, accounting for the decrease in magnitude of $\vec{B}_\mu$. Estimates for B_ℓ and B_t are dependent upon the lattice site, the local lattice distortion due to the presence of the muon, the shape and symmetry of the muon wave function, and upon changes in nearby iron moments produced by the muon. For a pointlike muon in an undistorted, unstrained lattice of unperturbed Fe moments B_ℓ($B_t = -1/2\ B_\ell$ here) is 18.5 (-5.21)kG at octa (tetra)-hedral sites.

If we use the displacements of lattice ions calculated by Sugimoto et al.[5] for the muon in Nb, B_ℓ in Fe reduces to 13.56(-3.73)kG at octa (tetra)-hedral sites for a point-like muon. In the $<B_d>$ calculations, the differences in elastic properties between Fe and Nb enter only in second order and will be ignored.

For a short-ranged, spherically-symmetric muon probability-density distribution the averaged B_ℓ will be the same as for a point-like muon at the site. However since the local site has only tetragonal symmetry we will take the form of the muon distribution as

$$|\psi_\mu(\vec{r})|^2 = \frac{1}{\alpha^2\beta\pi^{3/2}}\ e^{-\frac{x^2+y^2}{\alpha^2} - \frac{z^2}{\beta^2}}$$

for the site with the tetragonal axis parallel to $\vec{M}_s = M_s\hat{Z}$. Comparing the shape of the Gaussian type wave function and those calculated by Sugimoto

Table III

Magnetic dipolar fields under various conditions all at T = 0K.

		$4T(0)$	Site $_T$
1.	Point-like muon, rigid lattice	18.5	-5.2 kG
2.	Point-like muon, nearest neighbors relaxed according to scaling from Nb and V	13.5	-3.7 kG
3.	Spherical muon wave-function $\alpha = \beta = .15 - .19$ lattice relaxed as in 2.	13	-3.7 kG
4.	Oblate muon wave-function to match the general shape of a muon in Nb and V, $\alpha = .19, \beta = .15$	9.3	
5.	Prolate muon wave-function to match the T site shape in Nb and V, $\alpha = .19$, $\beta = .25$		-4.8 kG
6.	Point-like muon, lattice relaxed as in the calculations of Jena et al.	11.2	-4.4 kG
7.	Muon wave function as calculated by Jena et al. lattice relaxed as in 6.	7.6	-4.4
	$B_{dip}(T) = B_{dip}(0) \cdot M_s(T)/M_s(0)$ $M_s(0) = 1.750$ kG $M_s(300K) = 1.688$ kG $M_s(360K) = 1.658$ kG		
8.	$\delta(B_\ell + 2B_t)/100\mu\varepsilon$		
	Point-like muon	-7.1	-2.3 G/100με
	Calculated muon wave function and lattice relaxed	-2	-1

et al. for Nb, we estimate the value of α to be around 0.2 in units of the lattice parameter. Calculations have been performed varying α from 0.15 to 0.25 for the $^4T(0)$ octahedral site, and from 0.15 to 0.22 for the tetrahedral site. Geometric considerations suggest $\alpha \approx \sqrt{2}\,\beta$ for the $^4T(0)$ site and $\alpha \approx 1/\sqrt{2}\,\beta$ for the ^1T site.

Jena et al.[6] have calculated muon wave-functions and lattice displacements specific to the case of a muon in Fe. They also calculated the dipolar fields appropriate to their results, and these are presented in Table III as well as the change in $1/3(B_\ell + 2B_t)$ induced by strain.

Now to see whether eq. (1) is correct in the sense that the dominant effect which comes from the first term has the expected temperature dependence. We subtract the small final term from δB_μ obtaining:

$$\delta B'_\mu = +\,2/9\ (B_\ell - B_t)\Delta E/kT = \delta B_\mu - \frac{1}{3}\,(B_\ell + 2B_t)$$

The left side is proportional to $M_s(T)/T$, the saturation magnetization divided by the temperature. We thus expect that between 300K and 360K a ratio of $(M_s(300)/300)/(M_s(360)/360) = 1.22$, while the right side ratio using a weighting of 1:2 for octahedral to tetrahedral occupation, is: $(25.7 + 1.33 = 27)/(20.6 + 1.33 = 21.9) = 1.23$, in excellent agreement. Since $B_\ell \approx -2B_t$ we may write

$$\delta B'_\mu = 1/3\ B_\ell(0\ K)\ M_s(T)/M_s(0\ K)\ \Delta E/kT$$

Jena et al. have obtained $\Delta E = -.19$ meV and $+.53$ meV for the $^4T(0)$ and ^1T sites. Using these they obtain 18 and 29 G/100$\mu\varepsilon$ for the two sites. If again we assume equal occupation of these two types of sites, weighting them as 1:2 we obtain for the average shift 25.3 G/100$\mu\varepsilon$ which is certainly very close to the observed result of $27 \pm .5$ G/100$\mu\varepsilon$.

We can also extrapolate the results of Sugimoto and Fukai[5] on Nb and V to find the double force tensor diagonal elements for Fe in the two different types of sites. The extrapolation was linear in the lattice parameter observing that $P_1 - P_2$ changed by 5.3% and 9.7% for the 4T(0) and 1T sites respectively in their calculations upon decreasing the lattice parameter from 3.3A to 3.0A and then using the 2.87A lattice parameter of Fe.

Table IV

Site	$P_1 - P_2$ for 3.3A	$P_1 - P_2$ for 2.87A
4T(0)	3.466 eV	3.73 eV
1T	-1.075 eV	-1.23 eV

Since $\Delta E = ((S_{11} - S_{12})/S_{11}) \cdot (P_1 - P_2)\epsilon_{100}$ we find that ΔE is -.51 meV for the 4T(0) site and .17 meV for the 1T site. Using this ΔE and $B_\ell(0)$ which we calculate (9.3 kG for the 4T(0) site and -4.8 kG for the 1T site) we obtain the $\delta B_\mu'$ shown in Table V. We also include the results for the fields calculated by Jena et al. Since it is rather surprising that ΔE for the 4T(0) site is smaller in magnitude than that for the 1T site in the calculations of Jena et al. we finally present the results obtained upon reversing the ΔE though keeping the physically reasonable signs.

Table V.

$\delta B'_\mu$ in Gauss for room temperature, calculated under various conditions.

The average is for 1:2 weights for the 4T(0):1T sites.

	4T(0)		1T		Average
	$\delta B'_\mu$ G/100 με	ΔE(meV)	$\delta B'_\mu$ G/100 με	ΔE(meV)	$\delta B'_\mu$ G/100 με
Jena et al.[a]	18	.19	29	-.53	25.3
Extrapolate ΔE from Nb and V[b] fields from lines 4,5 of Table	61	.51	10.5	-.17	27.3
Extrapolate ΔE from Nb and V[b] fields from line 7 of Table	50	.51	9.6	-.17	23.0
Reversal of ΔE from Jena et al.[a]	51.8	.53	10.7	-.19	24.4
Experiment corrected for the small effects of dipole motion using the results of Jena et al.[a]					27±.5

[a] reference 6

[b] reference 5 and see text.

IV. Conclusions

We have determined that the precession frequency as a function of uniaxial strain for Fe arises primarily from symmetry breaking effects. The magnitude of the shift is reasonably well described by either the results of Jena et al.[6] or by extrapolation from the results of Sugimoto and Fukai[5] for Nb and V if one assumes in both cases that the muon occupies nearly equally the 4T(0) and 1T sites. This last is consistent with the results of Yagi et al.[7] and with the calculations for the energies of these sites, which are nearly equal. To be precise there is about a 30 MeV difference favoring the 4T(0) site in the calculations, but this is thought by Jena et al.[6] not to be significant.

The reduction of precession frequency with extension along <100> magnetization directions can explain the tendancy for cold worked iron samples to have reduced precession frequencies. Since magnetostriction in Fe favors domain alignment along the local directions of extension, the average precession frequency should thus be reduced.

That depolarization rates are evidently sensitive to internal strains and that these will become more important at lower temperatures imply that interpretations of depolarization rates which do not take these effects into account may need re-evaluation.

Similar frequency shifts associated with symmetry breaking should occur for those crystalline materials such as Fe_3Si or Fe_3Al which also have crystallographically equivalent potential muon sites which are magnetically inequivalent. Other systems, such as Ni, Co or Gd, though having only one

type of site, should have observable, if smaller, frequency shifts arising from the motion with stress of the crystal atoms and their associated dipole and hyperfine field distributions.

The effects of working the Fe samples which show up in irreversible frequency shifts, usually toward lower values, and depolarization rate increases have only been partially explored so far and will be reported later.

Acknowledgements

We would like to thank P. Jena and K. Petzinger for helpful discussions. This work was supported in part by NSF Grant DMR 8007059 and NASA Grant NSG 1342 and NAG1-416.

References

1. P. F. Meier, Hyperfine Inter. 8 (1981) 591.
2. K. Kanamori, H. Yoshida and K. Terakura, Hyperfine Inter. 8 (1981) 573.
3. T. Butz, J. Chappert, J. F. Dufresne, O. Hartmann, E. Karlsson, B. Lindgren, L. O. Norlin, P. Podini and A. Yaouanc, Phys. Lett 75A (1980) 321.
4. H. Kanzaki, J. Phys. Chem. Solids 2 (1957) 24.
5. H. Sugimoto and Y. Fukai, Phys. Rev. B22 (1980) 760.
6. P. Jena, M. Manninen, R. M. Nieminen and J. J. Puska, Phys. Rev. B29 (1984) 4170.
7. E. Yagi, G. Flik, K. Furderer, N. Haas, D. Herlach, J. Major, A. Seeger, W. Jacobs, M. Krause, H.-J. Mundinger and H. Orth, Phys. Rev. B30 (1984) 441 and E. Yagi, H. Bossy, K.-P. Döring, M. Gladisch, D. Herlach, H. Matsui, H. Orth, G. zu Putlitz, A. Seeger and J. Vetter, Hyperfine Inter. 8 (1981) 553.
8. R. A. Johnson, G. J. Dienes, and A. C. Damask. Acta Metall, 12 (1964) 1215.
9. C. E. Stronach, K. R. Squire, A. S. Arrott, B. Heinrich, W. F. Lankford, W. J. Kossler and J.J. Singh, Electronic Structure and Properties of Hydrogen in Metals, (P. Jena and C. B. Satterthwaite eds. Plenum, 1983) p. 617 and references therein.
10. J. Leese and E. Lord, Journal of Applied Physics 39 (1968) 8.
11. A. H. Morrish, The Physics Principles of Magnetism (John Wiley and Sons, New York, 1965).

12. B. A. Calhoun and W. J. Carr, Jr.: Pittsburgh Conference on Mag. and Magnetic Material (1955) p. 107 pub. by AIEE, 33 W. 39th Street NY. See also W. J. Carr, Jr. in the Encyclopedia of Physics, Volume XVIII/2 pub. by Springer Verlag (1966) p. 308.

Figure Captions

Figure 1 Three possible occupational configurations of interstitials in a bcc crystal.

Figure 2 μSR apparatus used at BNL. A very similar apparatus was used at SIN. The rectangle between the scintillators M5 and F6 represents the cryostat in which the pulling apparatus and sample were placed. The four crossed rectangles are the Helmholtz coils which produced the aligning field.

Figure 3 The pulling apparatus inside a vacuum chamber. The sample shown is the Fe(3wt%Si) which was 5 cm long and 1 cm wide. The grooves which were etched into the sample by electro-discharge machining are also indicated.

Figure 4 Muon precession frequency for (a) the Fe sample at 302 K and (b) the Fe(3wt%Si) sample at 300 K as a function of field applied along their long axes. Subsequent stress measurements were done using (a) 150 Oe or (b) 325 Oe.

Figure 5 The ratio F_t/F_ℓ for the Fe sample as a function of field applied along its long axis. F_t/F_ℓ is a measure of domain alignment. Subsequent stress measurements at 150 Oe had nearly complete domain alignment.

Figure 6 The depolarization rate Λ for the Fe(3wt%Si) as a function of applied field along its long axis. $P(t) = \exp(-\Lambda^2 t^2)$.

Figure 7 Muon precession frequencies for (a) Fe at 302 K, (b) Fe(3wt%Si) at 300 K, and (c) Fe(3wt%Si) at 360 K as functions of strain. The points immediately above the points along the falling straight lines were taken immediately after the lower points and had stress released. That they fall along horizontal lines indicates that we did not encounter irreversible, inelastic effects.

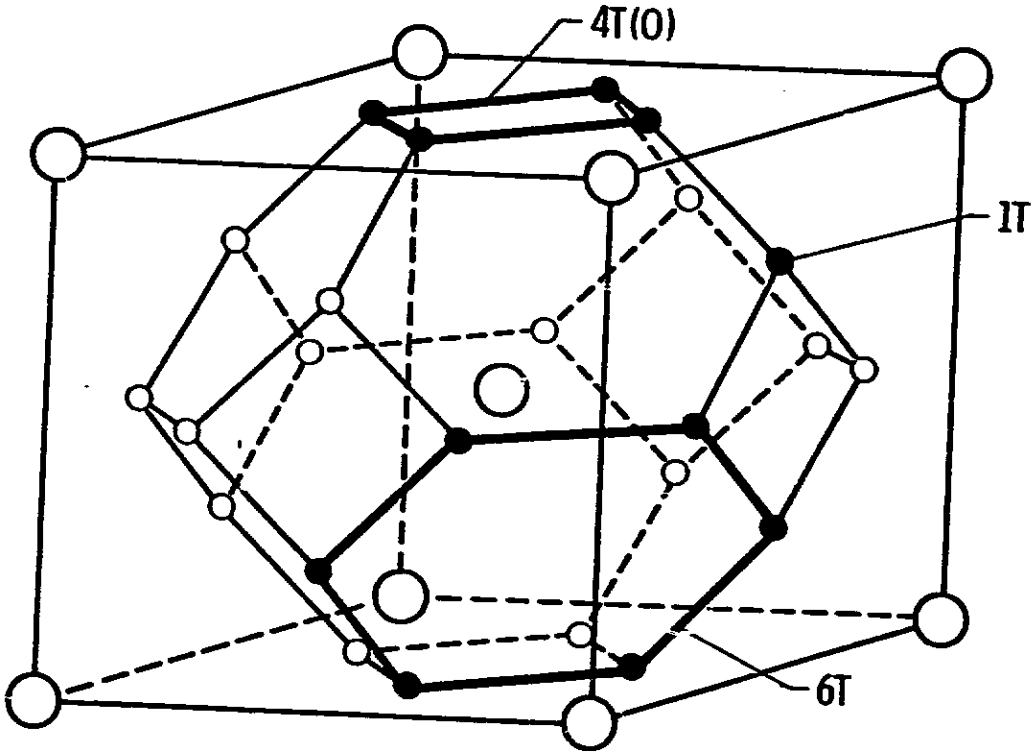

Fig. 1

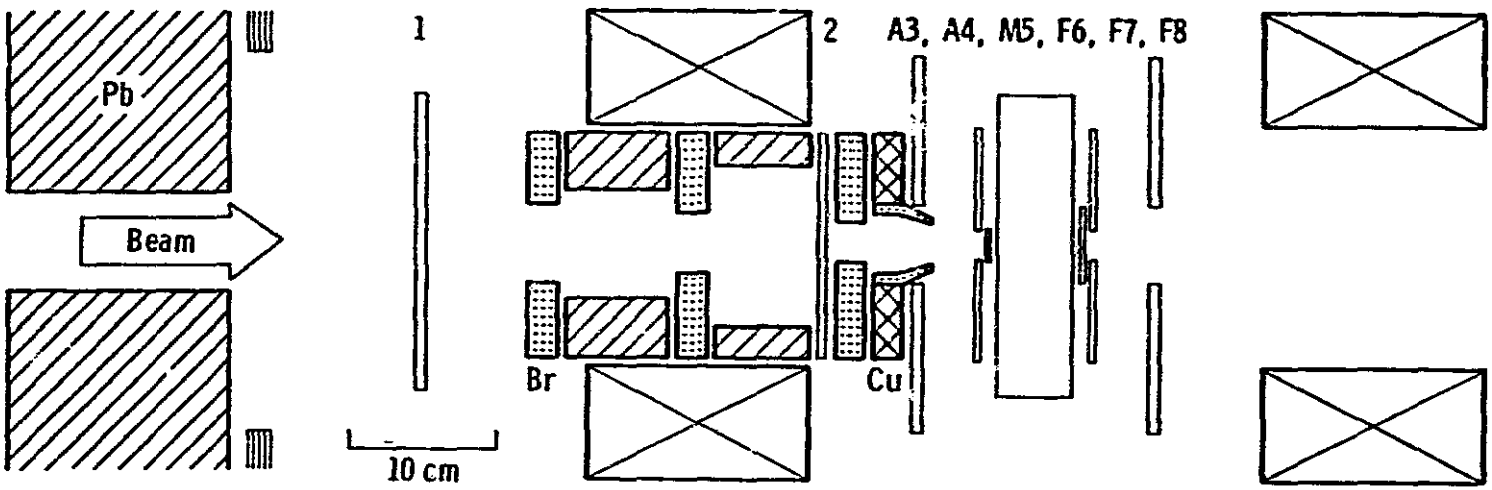

Fig. 2

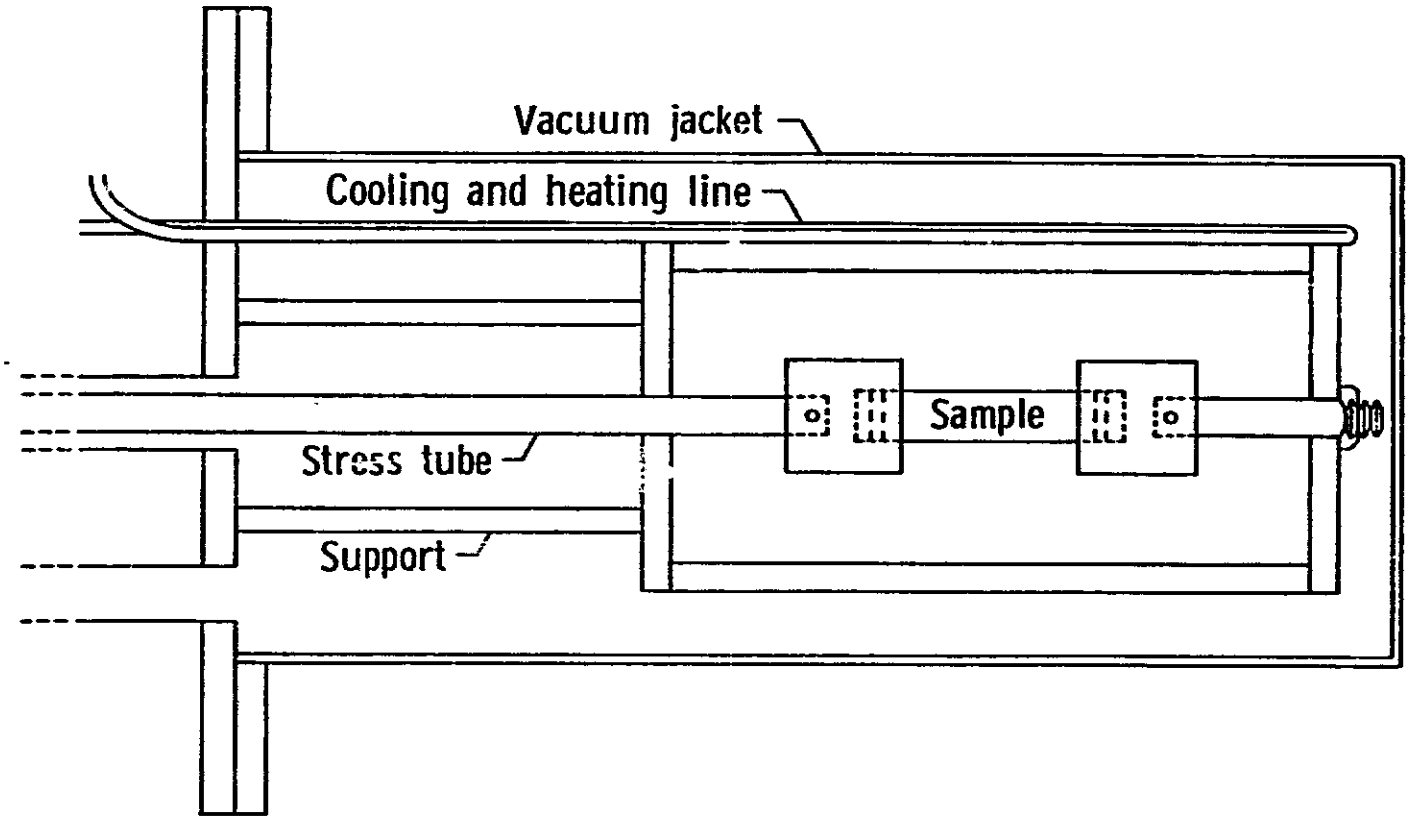
Vacuum jacket
Cooling and heating line
Sample
Stress tube
Support

Fig. 3

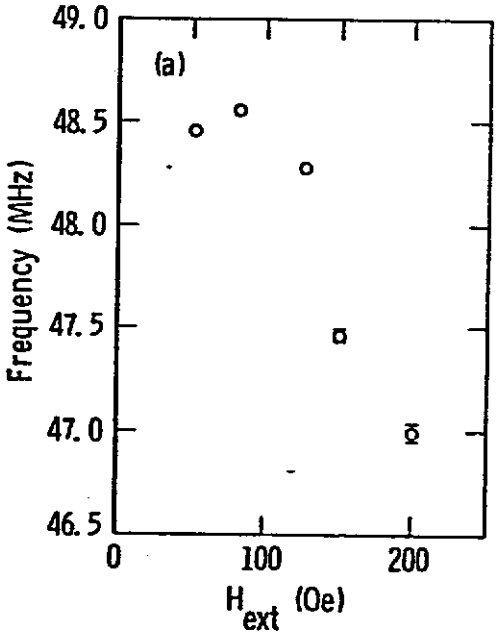
(a)
49.0
48.5
48.0
47.5
47.0
46.5
Frequency (MHz)
0
100
200
H_{ext} (Oe)

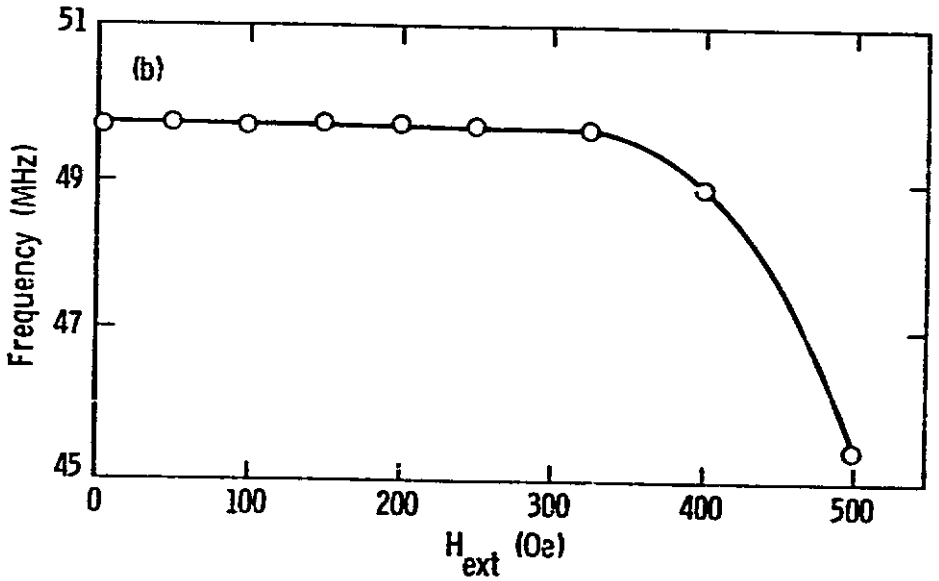
(b)
51
49
47
45
Frequency (MHz)
0
100
200
300
400
500
H_{ext} (Oe)

Fig. 4 (a) (b)

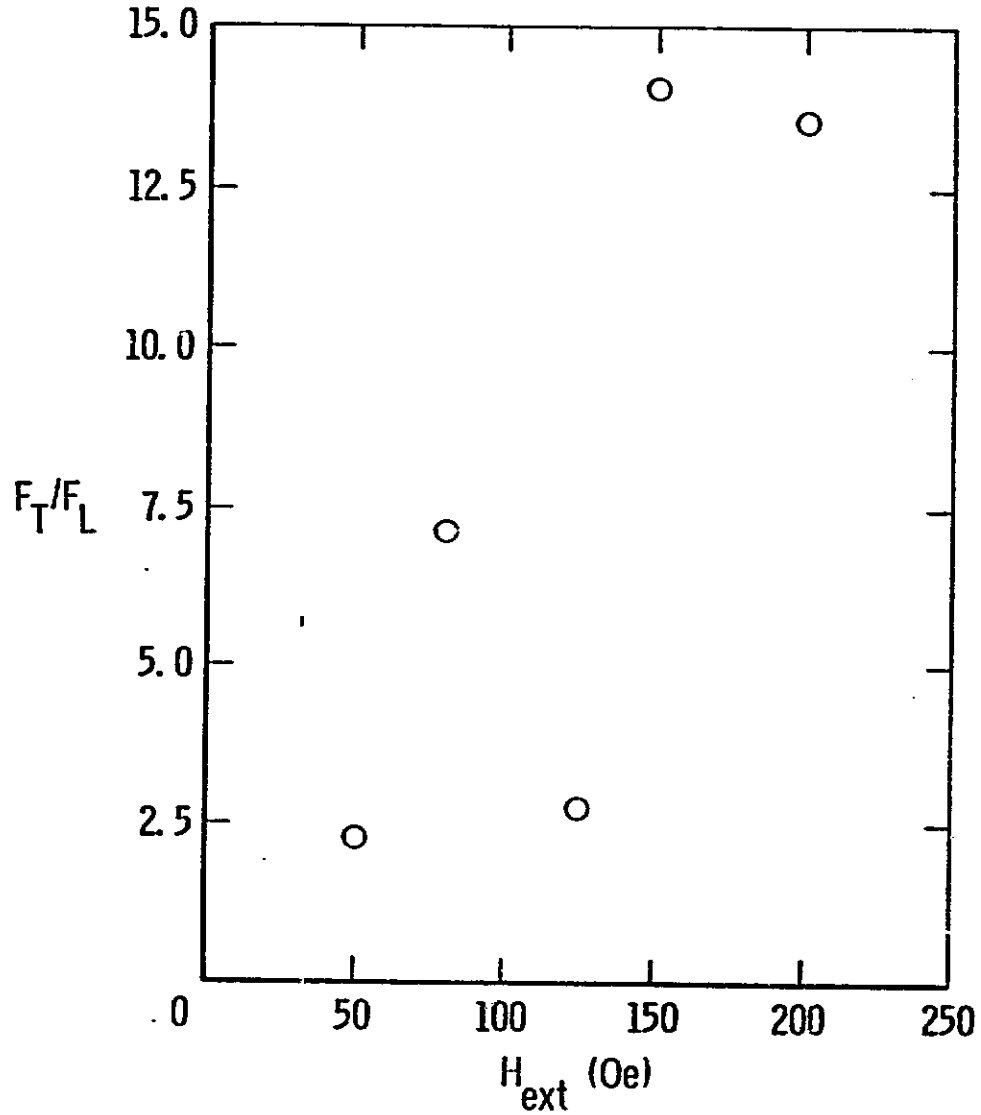

Fig. 5

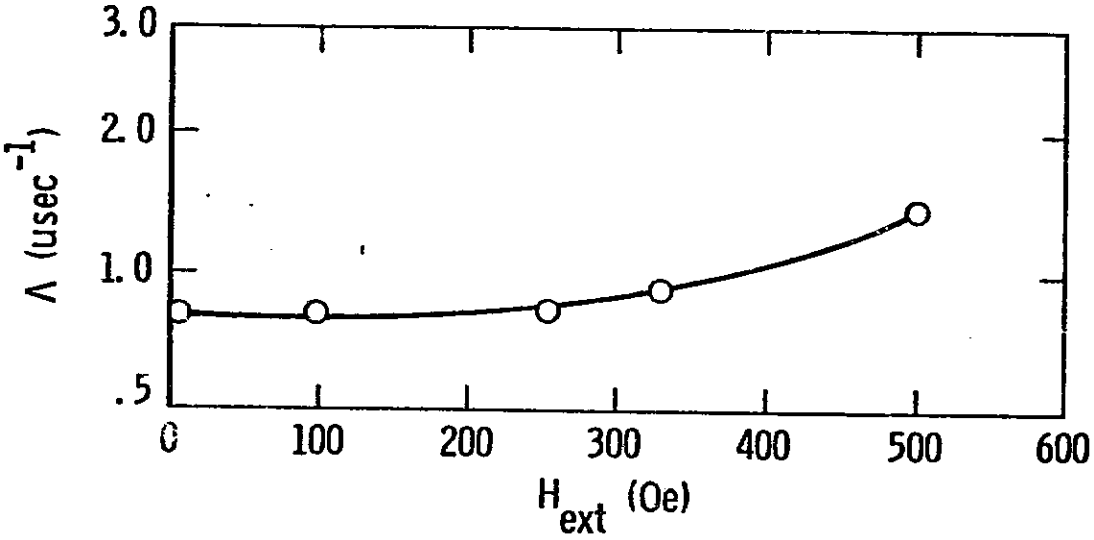

Fig. 6

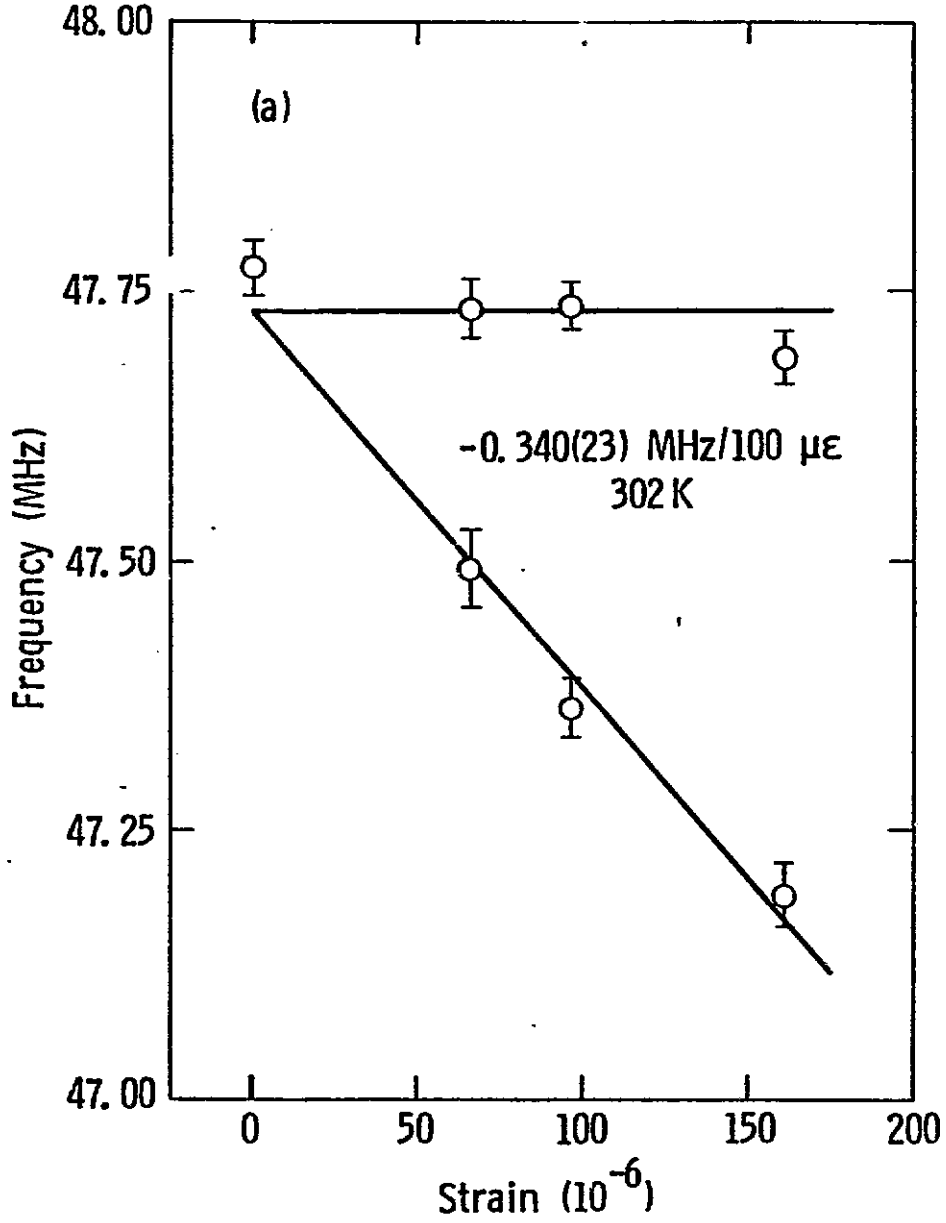
(a)
-0.340(23) MHz/100 με
302 K
Frequency (MHz)
Strain (10^{-6})
48.00
47.75
47.50
47.25
47.00
0
50
100
150
200

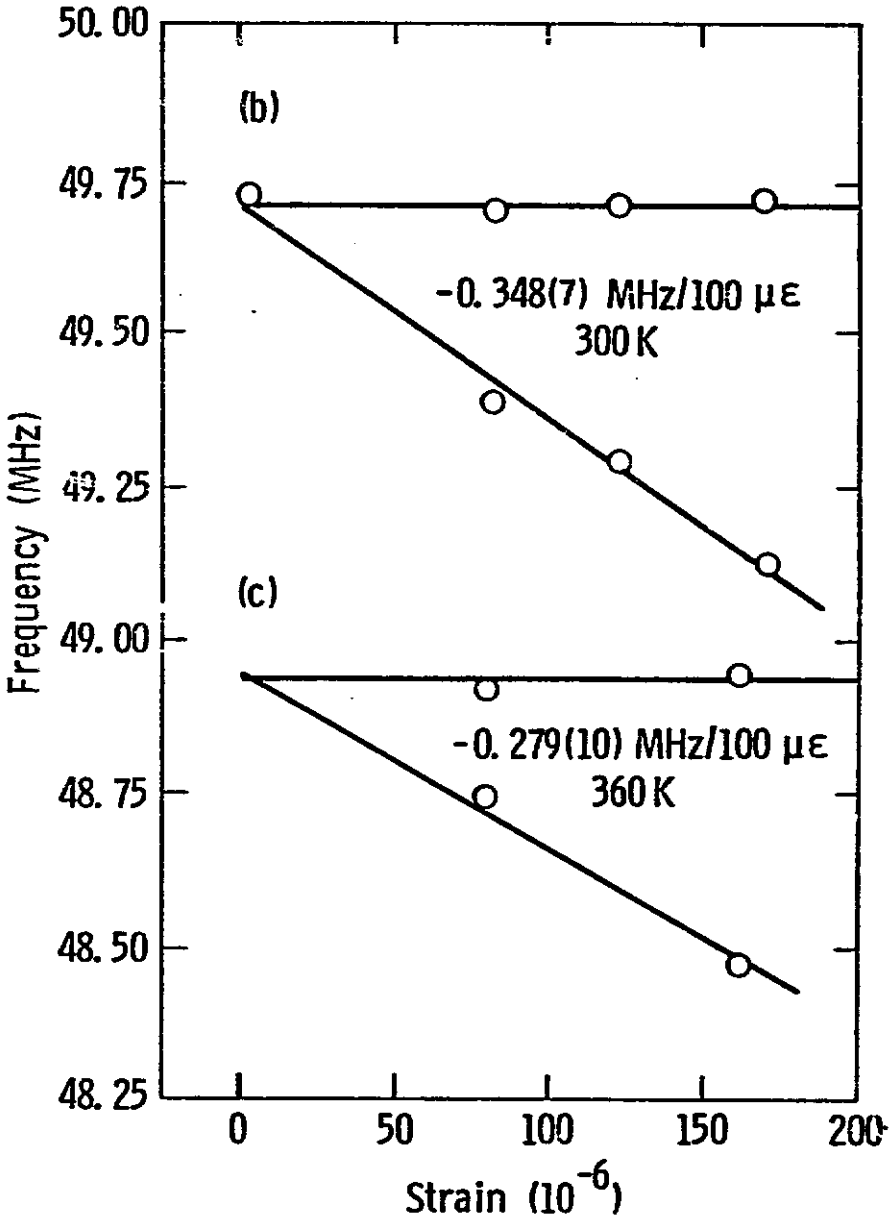
(b)
-0.348(7) MHz/100 με
300 K
(c)
-0.279(10) MHz/100 με
360 K
Frequency (MHz)
Strain (10^{-6})
50.00
49.75
49.50
49.25
49.00
48.75
48.50
48.25
0
50
100
150
200

Fig. 7 (a) (b)

D3

N85-28821

Pi(+)

200-MeV π^+ Induced Single Nucleon Removal from ^{24}Mg

Donald Joyce and Herbert O. Funsten
College of William and Mary
Williamsburg, VA 23185

B. Joseph Lieb
George Mason University, Fairfax, Virginia 22030

Hans S. Plendl and Joseph Norton
Florida State University, Tallahassee, Florida 32306

Carey E. Stronach
Virginia State University, Petersburg, Virginia 23803

V. Gordon Lind, Robert E. McAdams and O. Harry Otteson
Utah State University, Logan, Utah 84322

L. Wayne Swenson and Chandra Pillai
Oregon State University, Corvallis, Oregon 97330

David J. Vieira
Los Alamos National Laboratory
Los Alamos, New Mexico 87544

and

Anthony J. Buffa
California Polytechnic State University
San Louis Obispo, California 93401

Abstract

Nuclear γ-rays in coincidence with outgoing pions and/or protons following single nucleon removal from ^{24}Mg by 200 MeV π^+ have been detected with Ge(Li) detectors. Differential cross sections are reported for γ-rays from the first excited mirror states of ^{23}Na and ^{23}Mg in coincidence with positive pions and/or protons detected in particle telescopes at 30°, 60°, 90°, 120° and 150°; angle-integrated absolute cross sections and cross section ratios σ (^{23}Mg)/σ(^{23}Na) are calculated. These results are compared with the predictions of the one-step quasifree (OSQF), the intranuclear cascade (INC), and the nucleon charge exchange (NCX) reaction models. The OSQF and the INC calculations generally agree with the experimental results, while the NCX calculations are in disagreement.

PACS number: 25.80 HP

I. INTRODUCTION

The $(\pi,\pi N)$ reaction has been extensively studied using two general types of experiment. In one type of experiment, the residual nucleus or specific states of the residual nucleus are identified through radiochemical techniques [e.g. Ref.1,2], or via detection of prompt de-excitation γ-rays [e.g. Ref. 3]. Since no kinematical or angular information is obtained, these experiments integrate over both quasifree and non-quasifree components. In the other type of experiment [e.g. Ref. 4,5], the outgoing pion and/or proton is detected. With the proper geometry, the experimenter can select quasifree events; but only recently has the charged-particle energy resolution become sufficient to identify the final nuclear state. The present study includes features of both types of experiment by detecting prompt de-excitation γ-rays in coincidence with the outgoing pions or protons. It thus combines kinematic information with the ability to measure excitation of specific nuclear states. The principal motivation for this work was to better understand the mechanism of the $(\pi,\pi N)$ reaction, which is a valuable means of studying both nuclear structure and pion-nucleus reaction processes.

A feasibility study of the techniques employed in this work was undertaken at LAMPF using a single gamma ray detector in

coincidence with a single charged particle telescope [6]. The results of that study suggested the need to develop a large-scale coincidence measurement system sensitive to de-excitation gamma rays, knockout nucleons and scattered pions. Such an improved system was developed and used in the present work.

^{24}Mg was chosen as a target because single nucleon removal from ^{24}Mg results in the mirror nuclei ^{23}Mg and ^{23}Na. This provides a test of both single proton and single neutron removal mechanisms with pions. Furthermore, the single nucleon removal spectroscopic strengths (1 d $_{5/2}$ and 1 p $_{1/2}$) for ^{23}Na and ^{23}Mg from ^{24}Mg are concentrated in two low-lying excited states which γ-decay directly to the ground state [7]. For both ^{23}Na and ^{23}Mg, the first excited states ($\sim$0.45 MeV, $5/2^+$) have spectroscopic factors S^- of $\sim$ 4 - 6, and the $1/2^-$ excited states (at 2.64 MeV in ^{23}Na and at 2.77 Mev in ^{23}Mg) have spectroscopic factors of $\sim$ 4, as determined from the analysis of single-nucleon removal reactions on ^{24}Mg [7]. This yields an occupation number $C^2 S^- = 2$ for the $5/2^+$ levels, one-half the 1 d $_{5/2}$ shell limit of 4 in ^{24}Mg. (C is the isospin coupling coefficient, $(T_f \tau_f | 1/2 \tau_N | T_i \tau_i) = \sqrt{1/2}$.) Other bound excited states have considerably smaller spectroscopic factors. They predominantly feed the first excited state, but the combined effect of this γ-ray feeding should be less than 25% of the overall strength of the first excited state (if all states were populated in proportion to their spectroscopic factors).

The suitability of a ^{24}Mg target for $(\pi,\pi N)$ reaction work was established previously by the results of an inclusive study of γ-rays from $\pi^{\pm}$ reactions on ^{24}Mg conducted at SREL [3]. The two above-mentioned states in ^{23}Na and ^{23}Mg with large spectroscopic factors were strongly excited; there was no evidence for background γ-rays that might overlap these states. Another reason for the selection of a ^{24}Mg target was its suitability for a parallel study [8] of the angular correlation of γ-rays from (π,π') scattering.

II. EXPERIMENTAL APPARATUS AND PROCEDURES

The experiment was performed with a 300 MeV/c π^+ beam from the high-energy pion channel (P^3) of LAMPF. This beam had a contamination of 6.6% μ^+ and 2.0% e^+ as well as a muon halo of roughly three times the beam diameter in size. The beam spot size was typically 2.5 cm in diameter, and the momentum resolution was ~0.5%. The target consisted of natural magnesium metal (79% ^{24}Mg) with an average density of 0.57 ± 0.02 g/cm^2.

The experimental geometry consisted of six scintillation telescopes to detect charged particles and two Ge(Li) spectrometers to detect γ-rays (see Fig. 1). Each of the six particle telescopes consisted of the six NE 102 scintillators

(Π,Δ,E, Rear,Left-Side Veto, and Right-Side Veto). Each scintillator was coupled to a 5 cm photomultiplier tube, except for the E scintillator, which was coupled to two 12.5 cm photomultiplier tubes, one at each end. The detector thicknesses were 0.16 cm (Π), 0.32 cm (Δ), 0.635 cm (Veto and Rear scintillators), and 15.75 cm (E). The dimensions of each telescope component were the same for each telescope with the exception of the Π scintillators. The Π scintillators for telescopes 1, 5, and 6 at ± 30° and 150° had to be moved further from the target to avoid the beam halo; they were made correspondingly larger so that all the telescopes subtended the same solid angle.

The Π and Δ counters together defined the solid angle (~0.18 sr) for each telescope, and the E scintillator determined the particle energy. All three scintillators were used for particle identification. The Rear scintillator tagged particles which had not stopped in the previous scintillators. The two Side Veto scintillators tagged particles scattering out of or into the sides of the E scintillators. During off-line data analysis, however, this feature was not used in this experiment.

The six telescopes were placed on 30° centers from -30° to +150° (except at 0°) about the beam direction axis (see Fig. 1).

Calculation of the telescope solid angles was performed following the method of Gotch and Yogi [9], considering the size and location of the Π, Δ, and E scintillators for each telescope. All telescopes except number 6 were mounted together on a pivoting table with their axis directly under the target centerline. Telescope 6 was mounted on a similar, but smaller table pivoting on the same axis.

Two Ge(Li) γ-ray spectrometers were used in the present experiment, an Ortec 9% efficient and a Princeton Gamma-Tech 11% efficient lithium drifted germanium detector. Both detectors were fitted with NE 102 anti-coincidence scintillator cups to tag charged particles entering them. They were mounted on one rolling table to facilitate positioning and shielding. One detector was located at -75° and the other at +122° relative to the pion beam line axis (see Fig. 1). Additional experimental details are given in Ref. [8].

The beam intensity was monitored with a 7.6 cm thick ion chamber filled with argon, and the beam profile was monitored with a LAMPF wire chamber system [10]. The absolute cross sections were normalized to the differential inelastic π scattering cross sections from the 2^+ state of ^{24}Mg [11].

The six telescopes were calibrated in energy by tuning the channel for low-intensity protons at 50 MeV, 133 MeV and 191 MeV and placing each of the telescopes in the beam. The telescopes

were also calibrated with the pion and proton quasielastic scattering peaks from the experimental runs as well as with the maximum energy deposited in the E scintillators for pions and protons. The telescope calibration runs were also used to determine the efficiencies of the six telescopes. They were found to average 96 ± 2%.

The energy response of the two Ge(Li) detectors was periodically calibrated by placing ^{228}Th, ^{54}Mn, and ^{137}Cs sources at the target location. Well-known strong γ-ray peaks in the experimental data provided additional energy calibration, including the ^{24}Mg first-excited-state-to-ground transition and the ^{23}Na first-excited-state-to-ground transition. The maximum deviation of the calibration data from a linear fit was 0.7 keV, Relative and absolute Ge(Li) detector efficiencies were also determined in the source calibration runs.

A valid data event consisted of a coincidence between a particle telescope signal and a Ge(Li) γ-ray. For each event, pulse heights were digitized for Ω, Δ, E (two photomultipliers), and Rear scintillators as well as the Ge(Li) detectors. All data were read into a PDP-11 computer and written on magnetic tape for later replay.

Particles were identified from their Δ and E pulse heights using the method of Goulding *et al*, [12]. A particle which passed completely through the E scintillator (75 MeV pions and

160 MeV protons) as indicated by the Rear scintillator was treated using the method of England [13]. Fig. 2 shows a typical dE/dx vs. E dot plot (for Telescope 1, 30°), with the pions and protons identified.

During off-line data analysis, spectra were accumulated for γ-rays in one of the two Ge(Li) detectors that were in coincidence with pions or protons in any one of the six particle telescopes. Statistics were not sufficient to allow meaningful cuts on pion or proton energy. Fig. 3 shows the spectrum in the Ge(Li) detector at - 75° in coincidence with a pion or a proton in any one of the six telescopes. Fig. 4 shows the non-coincident spectrum for this detector.

The γ-rays in these spectra were identified by their energy, and areas were determined by summing channels and subtracting background. Cross sections were calculated from the relative areas and from the Ge(Li) and particle telescope efficiencies. As noted above, the cross sections were normalized to the ^{24}Mg 2^+ differential inelastic scattering cross sections of Bolger [11]. Major sources of error were the following: statistical errors and errors in the absolute normalization (~29%), Ge(Li) efficiency calibration (~9%), and telescope solid angle determination (~6%).

In addition to the strong first excited $5/2^+$ states at 0.439 MeV in ^{23}Na and 0.450 MeV in ^{23}Mg (see Fig. 3), there was

evidence for the fourth excited $1/2^-$ state in ^{23}Na at 2.64 MeV; but its Doppler-broadened width prevented a differential cross section measurement. There was no sign of its mirror state in ^{23}Mg. [Note that ^{23}Mg states were formed by either $^{24}Mg(\pi^+,\pi^+n)$ or $^{24}Mg(\pi^+,\pi^+p)$, and ^{23}Na states by $^{24}Mg(\pi^+,\pi^+p)$].

III. EXPERIMENTAL RESULTS; COMPARISON WITH REACTION MODELS

The experimental differential cross sections for production of the 0.439 and 0.450 MeV γ-rays in coincidence with outgoing pions or protons are listed in Table I for the two Ge(Li) detectors. The averages (last column of Table I) and the errors in the averages were weighted by the fractional errors in the cross sections. Where two cross sections differed greatly, the errors were increased in order to be more conservative. Data from Telescope 1 and 6 were averaged to give one data point at 30°.

The cross sections were extracted from the data by assuming isotropic γ-ray correlation with the outgoing pion or proton. This assumption would be rigorously true for direct plane wave nucleon knockout and can be seen to be approximately true within experimental uncertainties by comparing the relative cross sections of Ge(Li) 1 and 2 listed in Columns 4 and 5 of Table I. (Ge(Li) 1 and 2 had an angular separation of 50°.) This absence of angular correlation is in contrast to the expected strong

$\sin^2 2\theta_{\gamma q}$ correlation that was observed in this experiment (see Ref. [8]) for inelastic π^+ scattering to the 1.37 MeV first excited state of ^{24}Mg . ($\theta_{\gamma q}$ is the angle between the γ-ray and the inelastic momentum transfer direction.)

The above results were compared with predictions of an intranuclear cascade (INC) code developed by Fraenkel et al. [14] and with predictions of a simple plane wave impulse approximation which treats the reaction as one-step quasifree πN scattering (OSQF) and which includes the possibility of (incoherent) final-state nucleon charge exchange (NCX).

The INC predictions for the cross sections were based on $5 \cdot 10^4$ cascades of 200 MeV π^+ on ^{24} Mg. The program output was sorted to yield differential π^+ and cross sections at the angles measured in the present experiment for events in which the final nucleus was ^{23}Na or ^{23}Mg in a bound state. In performing these calculations, the part of the code that evaluates evaporation subsequent to the cascade was not used. Instead, a ^{23}Na or ^{23}Mg nucleus was assumed to retain its identity if its excitation energy following the cascade was less than its known particle stability energy. Of course, the INC code does not include details of nuclear structure or predict specific nuclear states. It has, however, no free parameters. The INC code calculates absolute pion and proton coincident cross sections to all bound states of the

residual nucleus. Contributions to the ^{23}Na/ ^{23}Mg bound states did not arise from only the nuclear surface (i.e. 1 $d_{5/2}$ shell nucleons). Hence, to compare the INC results to the experimental results, one should multiply the INC results by the ratio $r = \Sigma_{J^P} S^-(J^P) \cdot F(J^P, 5/2^+) / \Sigma_{J^P} S^-(J^P)$, where $S^-(J^P)$ is the spectroscopic factor for neutron or proton removal to a J^P ^{23}Na or ^{23}Mg bound state; $F(J^P, 5/2^+)$ is the relative amount of γ feeding from an initial J^P state down to the $5/2^+$ 1st excited state. Using spectroscopic factors and γ branching ratios from Ref. [7], $r = 0.6$ for both ^{23}Na and ^{23}Mg.

Analysis of the output from the INC calculation showed that a large fraction (~90%) of the cascades that produce a bound state of the A-1 residual nuclei are OSQF, with a monotonically decreasing population of residual states with increasing excitation energy.

The OSQF predictions for the cross sections were calculated using the semiempirical free πN phase shift of Rowe et al. [15]. The resulting cross sections were reduced, at small pion scattering angles, by Pauli blocking using a degenerate Fermi sphere uniformly filled up to a momentum of $k_F = 270$ MeV/c. This caused the resulting cross section at $\theta_\pi = 0°$ to be 0 and at $\theta_\pi \geq$~80° to approach the free π-N cross section. Nucleon Fermi motion was not included in the calculation. The reduced cross

section was then multiplied by the $1\,d_{5/2}$ proton or neutron occupation number for the first excited state, $C^2\,S^-_N = 2.2$, where C is the isospin coupling coefficient $(T_f\tau_f|1/2\tau_N|T_i\tau_i) = \sqrt{1/2}$ and S^-_N is the single neutron removal spectroscopic factor =4.2 [7]. It was necessary to scale the resulting cross section to the data by multiplying by a factor of ~1/3 - 1/5, which clearly indicates the predominance of other processes such as pion absorption and secondary scatterings.

Pion Angular Distributions

Figure 5 shows experimental and calculated angular distributions for outgoing pions that are in coincidence with γ-rays from the first excited states of ^{23}Mg and ^{23}Na. The solid curve represents the Pauli blocked OSQF results described above, the open circles are the results from the INC calculation. Without Pauli blocking, the pion differential cross section would rise steadily as θ decreases below ~60°. Both INC and OSQF calculations (and the data) display Pauli blocking with decreasing θ; the INC cross section falls off more rapidly than the OSQF cross section. An effect that could account for this discrepancy is nuclear shadowing of forward-scattered pions for the INC calculation. In the OSQF calculation, this effect has not been included.

Proton Angular Distributions

Fig. 6 displays the experimental angular distributions for outgoing protons in coincidence with γ-rays from the first excited states of ^{23}Mg and ^{23}Na, together with OSQF and INC results (solid curves and open circles, resp.). The angular distributions have the general shape of free π-N scattering, in which case no protons would be emitted at angles $\geq 90°$.

The E scintillator thickness (15 gm/cm^2) was insufficient to permit derivation of pion energy spectra but was adequate for determination of proton energy spectra by use of a fold-back procedure [8]. The 30° and 60° γ-coincident proton spectra are shown in Fig. 7. The arrows indicate the energies for free πN scattering ; the dashed lines indicate the INC results. Coincident proton spectra for $\theta_p \geq 90°$ had few total counts; as expected, no peak was observed. The spectra at 60° were corrected for a low-energy cutoff extending into the quasifree peak, as can be seen in Fig 7b.

IV. DISCUSSION OF RESULTS

The general shapes of both the pion and proton angular distributions coincident with γ-rays from the first excited $5/2^+$ states in ^{23}Mg and ^{23}Na were seen to be characteristic of free plane-wave πN scattering at the Δ resonance. The absolute values of the observed angular distribution cross sections, however, are

only 1/3 - 1/5 those expected from Pauli-blocked plane wave OSQF scattering on $1d_{5/2}$ nucleons with occupation numbers given by C^2S^- obtained from pick-up experiments [7]. However, due to the large free πN Δ-resonance cross section of 200 mb, the OSQF cross section approaches the geometrical (unitary) cross section for a ^{24}Mg nucleus. For proton knockout to the $5/2^+$ state of ^{23}Na, e.g., the OSQF cross section is ~280mb, which is comparable to the geometrical cross section, 450 mb. Our experimentally measured value is ~50 mb.

The large free πN Δ-resonance size represents an effective "swelling" of an individual nucleon to a size encompassing up to two adjacent nucleons leading to multiple or sequential π collisions that may predominate over OSQF. Furthermore, at the Δ resonance the effect even of small variations in the 600 mb non-elastic π - ^{24}Mg absolute cross section, which approximately equals the nuclear geometrical cross section, will cause correspondingly large variations in the calculated absolute cross section to ^{23}Mg and ^{23}Na, a component of the non-elastic cross section. Such variations, which depend upon pion multiple scattering and absorption, are only approximately calculated by the INC code. Hence, the INC calculation can be expected to give absolute ^{23}Na and ^{23}Mg cross sections which, although considerably closer to the data than OSQF, are still only approximate

(see Table II). Note that multiplication of the INC results in Table II by the factor r = 0.6 obtained in Section III yields cross section values that are about 1/3 the experimental ones.

From Fig. 5, the overall shapes of the differential cross sections from both INC and OSQF calculations are seen to agree with the π^+ coincident data, although at back angles the INC differential cross sections are substantially higher(lower) for ^{23}Na(^{23}Mg) than the OSQF and the experimental ones. At forward pion angles, Pauli blocking becomes predominant, considerably reducing the cross sections; e.g., at θ_π = 30° the free π^+N cross section is reduced by a factor of 2, based upon a model in which a uniformly filled sphere in momentum space has a Fermi surface at 270 MeV/c. This effect is also displayed by the INC results (see Fig. 5).

In view of the approximations used in the INC calculation, the agreement between the calculation and the data is good; it is within a factor of 2 of the agreement of a fit to the $^{12}C(\pi^\pm,\pi^\pm p)^{11}B$ data at T_π = 240 MeV by an INC calculation using a Fermi Gas momentum distribution for the nucleons [16].

The ratios $\sigma_\pi(^{23}Na)/\sigma_\pi(^{23}Mg)$ for the π^+ coincident differential cross sections have values of ~ 4, approximately independent of θ_π (see Table I). This is in disagreement with the results of Kyle

et al. [5] at T_π = 240 MeV in which the corresponding charge ratio $R = \sigma[\pi^+p/\pi^-p]$ for $^{16}O(\pi^\pm,\pi^\pm p)^{15}N_{g.s.}$ reaches a very large value, $R > 30$, for forward angles, $\theta_p \sim 35°$. Kyle et al. suggest that this enhancement over the quasifree value of 9 comes from a reduction in the the π^-p cross section, as π^+p enhancement is unlikely. In our experiment, however, the angle-integrated π^+ coincident ^{23}Mg $5/2^+$ cross section, which corresponds to the π^-p cross section of Kyle et al., is relative to OSQF the largest of all four measured cross sections (see Table II, Column 7). It may be noted that the enhancement found by Kyle et al. occurs at scattering angles where Pauli blocking is predominant.

The p coincident differential cross section comparison (Fig.6) is more ambiguous since there are only two data points (θ_p = 30°,60°) having values appreciably larger than zero (see Table I). (Free πN scattering yields no recoil protons at $\theta_p^{lab} > 90°$).

Our π^+ and p coincident ^{23}Na cross sections are equivalent to the $^{12}C(\pi^+,\pi^+p)$ results of Piasetzky et al. [4] who used a double spectrometer arm system. Their cross section values approximately equal those for free π^+p scattering; and assuming that four p shell protons are available , their effective participation ratio is approximately 0.25, which agrees with our results for ^{23}Na (Table II, Column 7). However, their $^{12}C(\pi^-, \pi^-p)$ cross section is ~60% greater than our equivalent π^+ coincident ^{23}Mg cross section.

There are large single nucleon removal spectroscopic factors for the $^{23}Na/^{23}Mg$ $1/2^-$ mirror states near 2.7 MeV, with $S^-(1/2^-) \approx S^-(5/2^+)$ [7]. The results of an earlier $\pi^{\pm} + {}^{24}Mg$ γ-ray experiment [3] in which a π coincidence was not required, were $\sigma(1/2^-) \approx 0.5\sigma(5/2^+)$ in rough agreement with the spectroscopic strengths. In the present experiment, however, $\sigma(1/2^-) < 0.1\ \sigma(5/2^+)$ was observed. This difference may be due to the peripheral nature of the interaction; the π^+ coincidence required in the present experiment may make the interaction appear more peripheral than the earlier singles experiment. However, the INC calculations do not yield contributions to ^{23}Na, ^{23}Mg bound states that arose from only the nuclear surface with which to make comparisons.

An examination of the particle histories generated by the INC code yields the following further information on the $^{24}Mg(\pi,\pi p)$ reaction:

A. INC predicts total, elastic, and absorption cross sections of 980, 400, and 230 mb, resp., in general agreement with 960,380 and 218 mb, resp., as measured by Ashery et al. [17] for 245 MeV $\pi^+ + {}^{27}Al$.

B. INC indicates that 75% of the Δ's decay before striking a nucleon. This is due to the short free decay length of the Δ (~0.4 f). An OSQF calculation indicates that

Pauli blocking of the decay is not predominant - only ~1/3 of the Δ decays are Pauli-blocked.

C. According to the INC results, pions from Δ decay predominantly do not escape the nucleus; 75% of the pions from Δ decay strike a nucleon to re-form another Δ. Using the Δ decay probability given above in B, this yields an average of two sequential Δ's formed for each T = 200 MeV pion incident on the nucleus. In an OSQF scattering process, the pion loses an average of 60 MeV lab kinetic energy; after two or more pion scatterings through Δ formation, T_π will have dropped considerably below resonance energy. INC yields a pion scattering mean free path of 1.2 f; c.f.

$\lambda = \frac{1}{\rho\sigma_{\pi\ \text{total}}}$ = 2.3 f for ^{24}Mg. (Pion absorption occurs only through ΔN → NN).

D. INC indicates that approximately 70% of the protons resulting from Δ decay escape the nucleus without further scattering. INC yields λ_p = 4.5 f; this is in agreement with $\lambda_p = 1/\rho\sigma_p$ > 5 f obtained from free, but Pauli blocked [18] NN total cross sections [19] and a ^{24}Mg uniform nuclear matter density ρ of radius 1.315 f [20]. The INC result is also in agreement with estimates by Schiffer [21].

Approximately half of the non-escaping protons undergo charge exchange before escaping in the INC calculations.

E. Approximately 40% of the total cross section for incident pions results in pion capture (ΔN-NN), according to the INC calculation. Measurements by Ashery et al. [17] indicate a ratio of capture-to-total cross section of ~30%.

The above INC results indicate that pion multiple scattering, occurring mainly by sequential Δ production and decay, is a predominant process, being more important (λ_π = 1.2 f) than nucleon multiple scattering (λ_p = 5 f) which was proposed some time ago [22] as a major process in pion-induced nucleon knockout at Δ resonance energies. In that process, the nucleon from Δ decay undergoes subsequent incoherent nuclear scattering with a probability of nucleon charge exchange (NCX) P ≈0.1 - 0.2 [22], as determined from charge exchange cross section ratios obtained in an activation experiment, $\sigma[^{12}C(\pi^+,X)\ ^{11}C]/\sigma[^{12}C(\pi^-,X)^{11}C]$ [1]. In the present experiment, both π^+ and p coincident cross sections for de-excitation γ-rays are determined. Hence the present experiment provides a more sensitive test of the NCX model than the previous activation experiments, which sum over these two final states.

The NCX calculation predicts the cross sections for the final

states $^{23}Mg + \pi^+$, $^{23}Mg + p$, $^{23}Na + \pi^+$, and $^{23}Na + p$ to be in the ratio of (1+9P):2:(9+P):(9+P). Since the ^{23}Na residual nucleus must be accompanied by both π^+ and p, the final states $^{23}Na + \pi^+$ and $^{23}Na + p$ must have the same cross sections regardless of the reaction model. Hence, the two experimental ^{23}Na cross sections (see Table II) were averaged, yielding $\sigma[^{23}Na(Av)] = 48$ mb. There are then only two independent cross section ratios. Let them be the ratios of $\sigma[^{23}Mg + \pi^+]$ and $\sigma[^{23}Mg + p]$ to $\sigma[^{23}Na(Av)]$. The first ratio, $R_1 = \sigma[^{23}Mg + \pi^+]/\sigma[^{23}Na(Av)] = 0.23$, yields $P \approx 0.12$, consistent with values of P obtained from activation work. (Quasifree $R_1 = 1/9$.) However, the second ratio, obtained from the proton component of the ^{23}Mg final state, has a value $R_2 = \sigma[^{23}Mg + p]/\sigma[^{23}Na(Av)] \approx 0.33$, yielding a large negative value of P, $P \approx -3$, which is, of course, inconsistent with NCX. (Quasifree $R_2 = 2/9$.)

A comparison of our experimental results with the results of activation measurements can be made by summing the measured π^+ and p components of the ^{23}Mg cross section (see Table II). This yields a ratio $\sigma[(^{23}Mg + \pi^+) + (^{23}Mg + p)]/\sigma[^{23}Na(Av)] \approx 0.56$, which in turn yields a value of $P \approx 0.24$, consistent with the value of P obtained from activation measurements.

The above results indicate that whereas the INC model can explain inclusive cross section results such as those obtained by

activation measurements, it is inconsistent with the more exclusive cross sections obtained in the present experiment. This conclusion agrees with calculations of Karol [23], which indicate a small probability for NCX (~3%).

In a recent paper, Ohkubo and Liu [24] include the effects of quantum-mechanical interference between quasifree and non-quasifree (NCX and πCX) reaction processes using distorted waves. Their calculations result in significantly better agreement with the experimental results for $^{12}C(\pi^+,\pi N)^{11}C$ cross section ratios [1] than the previously incoherent NCX calculations [22]. In a subsequent paper [2], Ohkubo, Liu et al. conclude that both NCX and the interference effects decrease considerably in magnitude as the target mass is increased from A = 12. Their results suggest that these effects are small for an A = 24 target.

A process in which an initial Δ subsequently interacts with a nucleon in a $(\Delta N)^{T=2}$ state, interestingly, reproduces the measured values of R_1 and R_2. Such a process, in which one of the $(\Delta N)^{T=2}$ decay nucleons subsequently remains in the nucleus, yields $R_1 = 0.22$ and $R_2 = 0.37$, i.e. values close to those observed.

Although there has been evidence for a possible $(\Delta N)^{T=2}$ attractive potential [25], an examination of the magnitude of pion double charge exchange cross sections casts doubt on this process. Even after allowing for isospin recoupling, which yields for pion

double charge exchange a $(\Delta N)^{T=2}$ component $\sim 1/3$ that of a $(\Delta N)^{T=1}$ component, any ΔN contribution that is sufficiently large to yield a reasonable $(\pi,\pi N)$ reaction would result in a pion double charge exchange cross section too high by at least a factor of 10.

V. CONCLUSION

The experimentally determined differential cross sections of de-excitation γ-rays from the $5/2^+$ first excited states of ^{23}Na and ^{23}Mg in coincidence with outgoing π^+ and/or p from ^{24}Mg$(\pi^+,\pi N)$, the corresponding angle-integrated absolute cross sections, and the cross section ratios $\sigma(^{23}\text{Mg})/\sigma(^{23}\text{Na})$ have been compared with the results of calculations based on several $(\pi,\pi N)$ reaction models, in particular on the plane-wave one-step quasifree (OSQF) and the intranuclear cascade (INC) model, and on charge exchange of the outgoing nucleon (NCX).

Both the OSQF and the INC calculations reproduce the approximate shape of the observed π^+ and p angular distributions. The INC calculations, which can be considered absolute, agree with the absolute measured angle-integrated cross sections within a factor of ~ 2. These calculations indicate that rescattering of the outgoing pions is a more important process than interactions of the outgoing nucleons. The NCX model is put to a more sensitive test by the present experiment than by previous activation

experiments, since π^+ and p coincident cross section ratios for de-excitation γ-rays are determined separately rather than together. The NCX results are inconsistent with experimental results.

These comparisons with several reaction models suggest that a more detailed description of the πN interaction in a nucleus, such as the Δ-hole model of Hirata, Lenz and Thies. [26], may be needed for a better understanding of the processes involved in the $(\pi,\pi N)$ reaction.

ACKNOWLEDGMENTS

We wish to thank Jean Julien, Herbert O. Funsten III and David C. Plendl for their participation in the data collection, Peter Gram for valuable discussions on experimental details, and Robert Damjanovich and other members of the LAMPF staff for technical assistance. This work was supported in part by the NSF; the participation of one of us (C.E.S.) was also supported in part by NASA.

References

1. B. J. Dropesky, G. W. Butler, C. J. Orth, R. A. Williams, M.A. Yates-Williams, G. Friedlander and S. B. Kaufman, Phys. Rev. C 20 1844 (1979).

   L. H. Batist, V. D. Vitman, V. P. Koptev, M. M. Makarov, A. A. Naberezhov, V. V. Nelyubin, G. Z. Obrant, V. V. Sarantsev, and G. V. Scherbakov, Nucl. Phys. A254, 480 (1975).

2. Y. Ohkubo, C. J. Orth, D. J. Vieira, and L. C. Liu, Phys. Rev. C (scheduled for publication).

3. B. J. Lieb, H. S. Plendl, C. E. Stronach, H. O Funsten and V. G. Lind, Phys. Rev. C19, 2405 (1979).

4. E. Piasetzky, D. Ashery, A. Altman, A. J. Yavin, F. W. Schleputz, R. J. Powers, W. Bertt, L. Felawka, H. K. Walter, R. G. Winter, and J. Van Der Pluym. Phys. Rev. C25, 2687 (1982).

5. G. S. Kyle, P.- A. Amandruz, Th. S. Bauer, J. J. Domingo, C. H. Q. Ingram, J. Jansen , D. Renker, J. Zichy, R. Stamminger, and F. Vogler, Phys. Rev. Lett. 52, 974 (1984)

6. V. G. Lind, R. E. McAdams, O. H. Otteson, W. F. Denig, C. A. Goulding, M. Greenfield, H.S. Plendl, B. J. Lieb, C. E. Stronach, P. A. M. Gram and T. Sharma. Phys. Rev. Lett. 41, 1023 (1978).

7. P.M. Endt and C. Van der Leun, Nucl. Phys. A310, (1978).

8. D. Joyce, Positive Pion Scattering on ^{24}Mg. Ph.D. Thesis, College of William and Mary (1982).

9. H. Gotch and H. Yogi, Nucl. Inst. Methods 96, 485 (1971).

10. G. J. Krause and P. A. M. Gram, Nucl. Inst. Methods, 156 265 (1978).

11. J. Bolger, private communication (1979).

12. F. S. Goulding, D. A. Landis, J. Cerny, and R. H. Pehl, Nucl. Inst. Methods, 31 , 1 (1964).

13. J.B.A. England, Techniques in Nuclear Structure Physics, Part2, p. 419, John Wiley and Sons (1974).

14. Z. Fraenkel, Phys. Rev. 130, 2407 (1963); G. D. Harp, K. Chen, G. Friedlander, Z. Fraenkel, and J. M. Miller, Phys. Rev. C8, 581 (1973).

15. G. Rowe, M. Salomon, and R. H. Landau, Phys. Rev. C18 584 (1978).

16. Z. Fraenkel, E. Piasetzky, and G. Kalberman, Phys. Rev. C26 1618 (1982).

17. D. Ashery, I. Navon, G. Azuelos, H. J.Pfeiffer, H. K. Walter, and F. W. Schlepütz, Phys. Rev. C23, 217 (1981).

18. K. Kuckuchi and M. Kawai, Nuclear Matter and Nuclear Reactions, North Holland (1968).

19. W. N. Hess., Rev. Mod. Phys. 30 368 (1968).

20. Landolt and Bernstein.

21. J. P. Schiffer, Nucl. Phys. A335 339 (1980).

22. M. M. Sternheim and R. R. Silbar, Phys. Rev. Lett. 34, 824 (1975).

23. P. J. Karol, Phys. Rev. C23, 415 (1981).

24. Y. Ohkubo and L. C. Liu, Phys. Rev. C30, 254 (1984).

25. H. Toki, private communication.

26. M. Hirata, F. Lenz, and M. Thies , Phys. Rev. C28, 785 (1983).

Figure Captions

1. Experimental Geometry. The rear and side veto counters surrounding each E counter are shown but not labelled.
2. A dE/dx vs. E dot plot for Telescope 1 at 30°. The E signal was from one of the two photomultipliers of that scintillator.
3. Ge(Li) 1 γ-ray spectrum in coincidence with a π^+ or p from $^{24}Mg(\pi^+,\pi N)$ in any one of the six particle telescopes (low-energy portion).
4. Ge(Li) 1 γ-ray spectrum with no coincidence required (low-energy portion).
5. Differential cross sections of outgoing π^+ from $^{24}Mg(\pi^+,\pi^+N)$ in coincidence with γ-rays from the first excited states of ^{23}Na and ^{23}Mg compared with one-step quasifree (OSQF) and intranuclear cascade (INC) calculations. OSQF values have been multiplied by 0.20 for ^{23}Na and by 0.38 for ^{23}Mg.
6. Differential cross sections of protons from $^{24}Mg(\pi^+,\pi p)$ in coincidence with γ-rays from the first excited states of ^{23}Na and ^{23}Mg compared with one-step quasifree (OSQF) and intranuclear cascade (INC) calculations. OSQF values have been multiplied by 0.17 for ^{23}Na and by 0.28 for ^{23}Mg. OSQF and INC values at backward angles are <0.1 mb/sr and hence do not show up on the semi-log plot.

7. Energy spectra of protons from $^{24}Mg(\pi^+,\pi p)$ detected at 30° and 60° in coincidence with γ-rays from the first excited states of ^{23}Na and ^{23}Mg compared with INC calculations (dashed line). The arrows indicate the energies for free πN scattering.

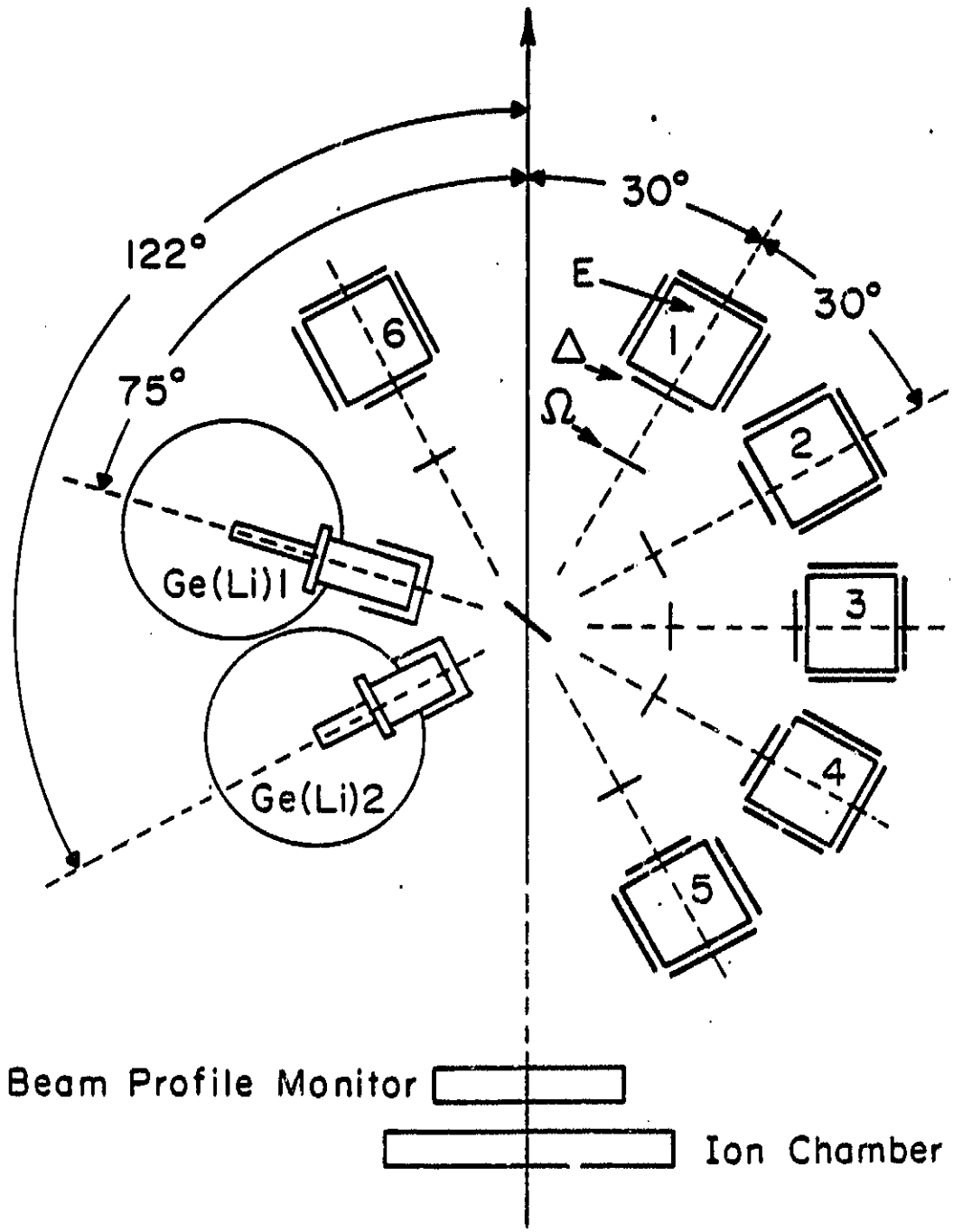
122°
30°
30°
75°
E
Δ
Ω
1
2
3
4
5
6
Ge(Li)1
Ge(Li)2
Beam Profile Monitor
Ion Chamber

Fig. 1

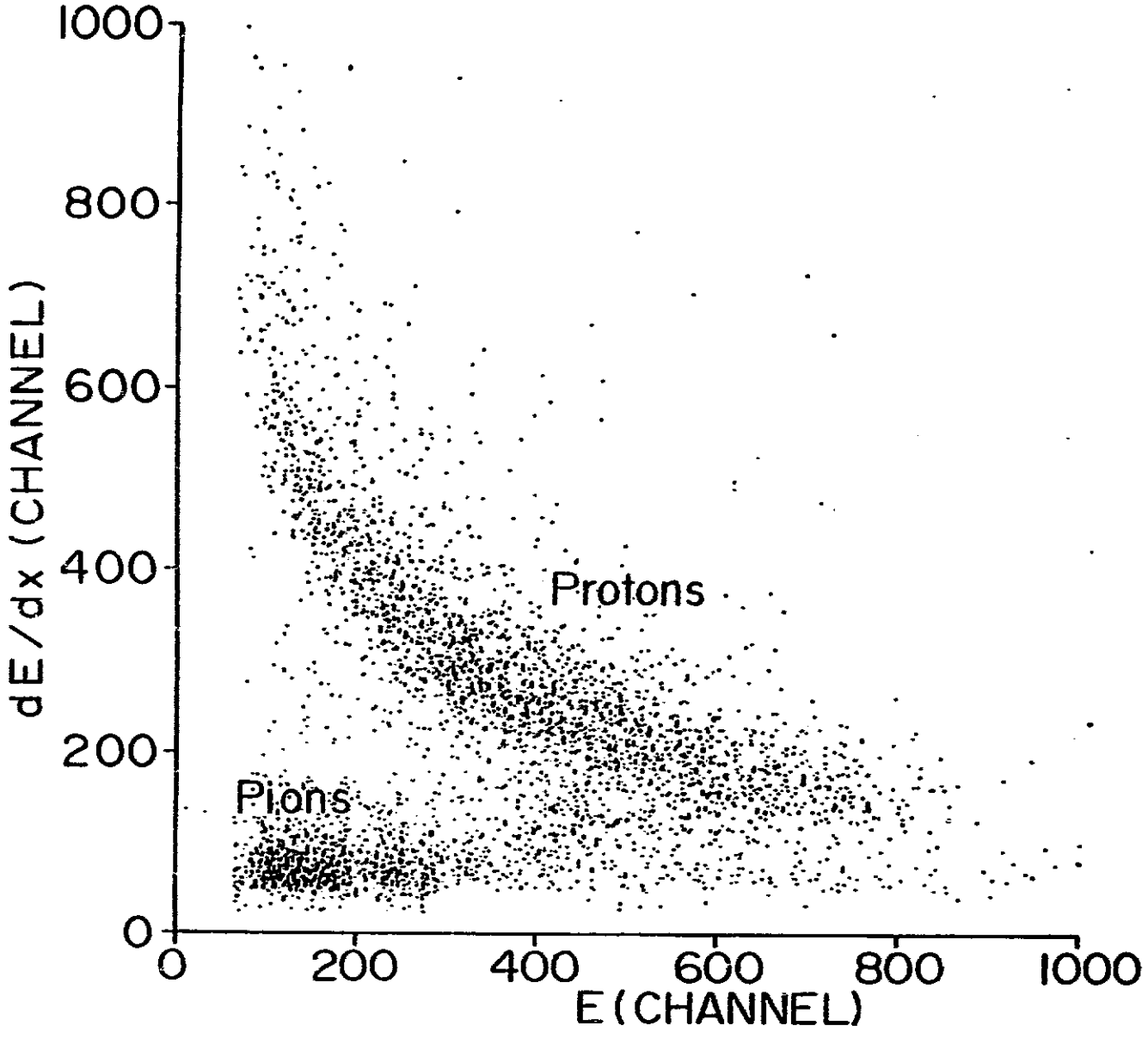
1000
800
600
400
200
0
dE/dx (CHANNEL)
Protons
Pions
0
200
400
600
800
1000
E (CHANNEL)

Fig. 2

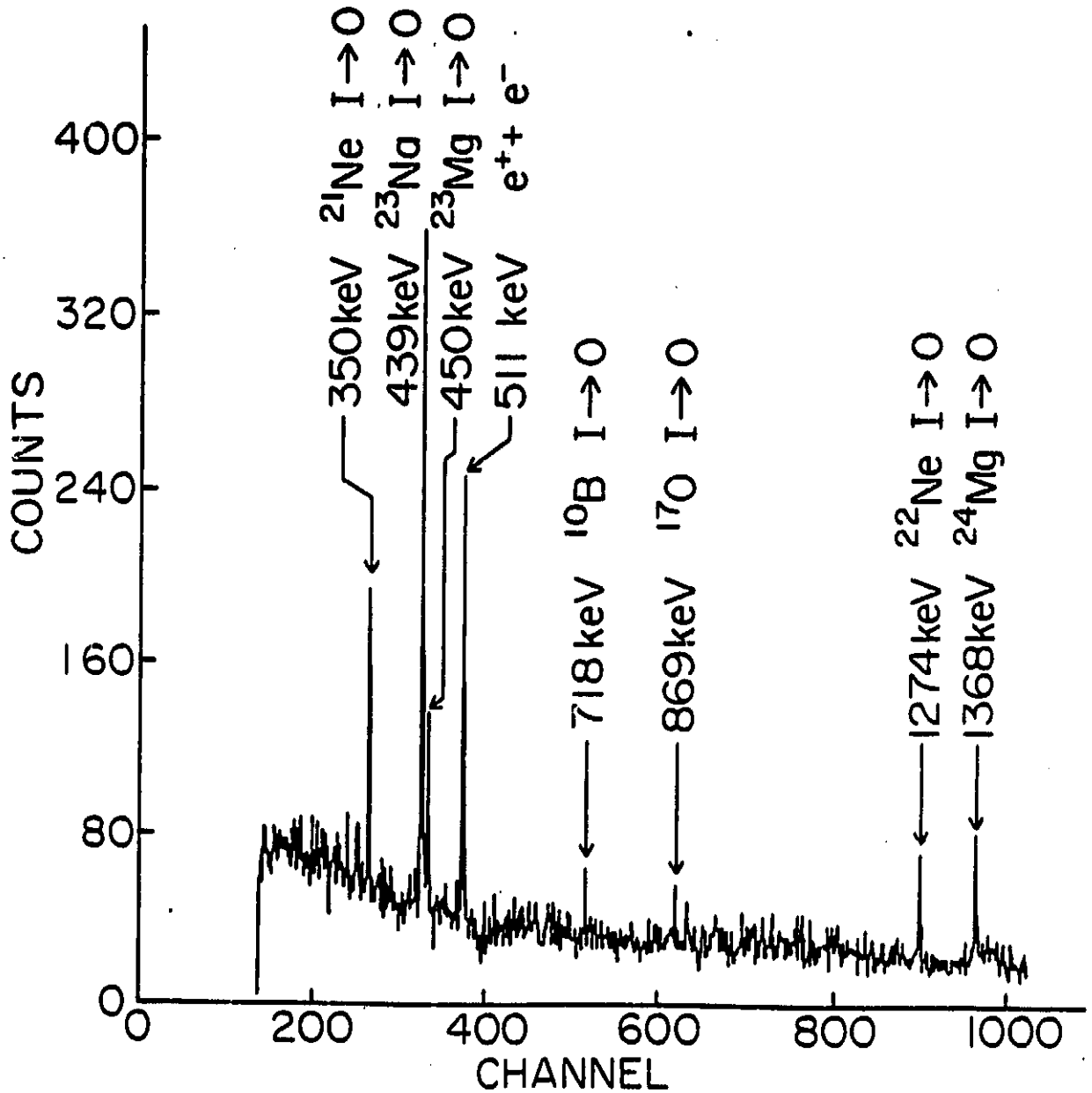
COUNTS
400
320
240
160
80
0
0
200
400
600
800
1000
CHANNEL
350keV ^{21}Ne I→0
439keV ^{23}Na I→0
450keV ^{23}Mg I→0
511 keV e$^+$+ e$^-$
718keV ^{10}B I→0
869keV ^{17}O I→0
1274keV ^{22}Ne I→0
1368keV ^{24}Mg I→0

Fig. 3

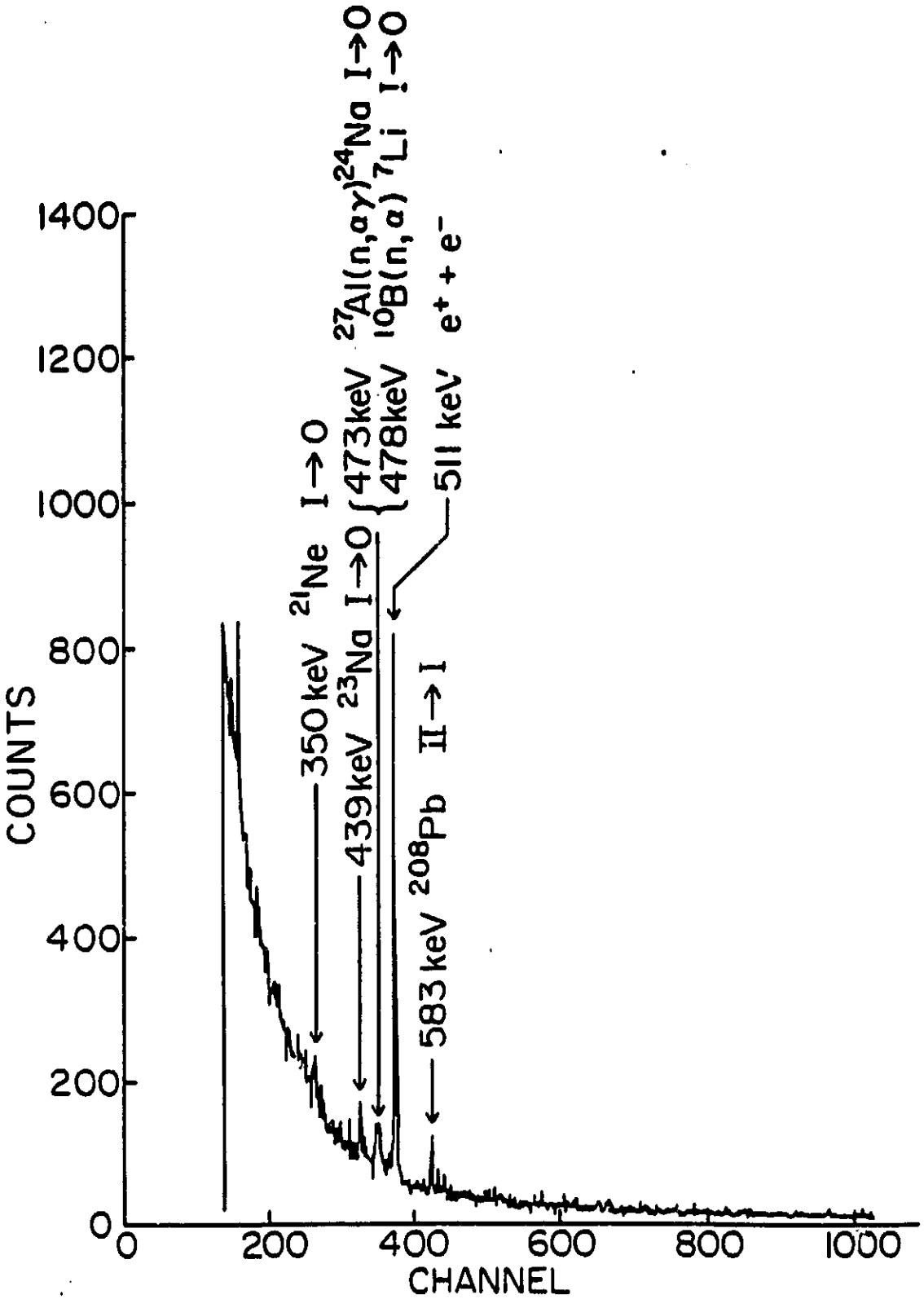
COUNTS
CHANNEL
0
200
400
600
800
1000
1200
1400
350 keV ^{21}Ne I→0
439 keV ^{23}Na I→0
583 keV ^{208}Pb II→I
473 keV ^{27}Al(n,αγ)^{24}Na I→0
478 keV ^{10}B(n,α)^{7}Li I→0
511 keV e$^+$ + e$^-$

Fig. 4

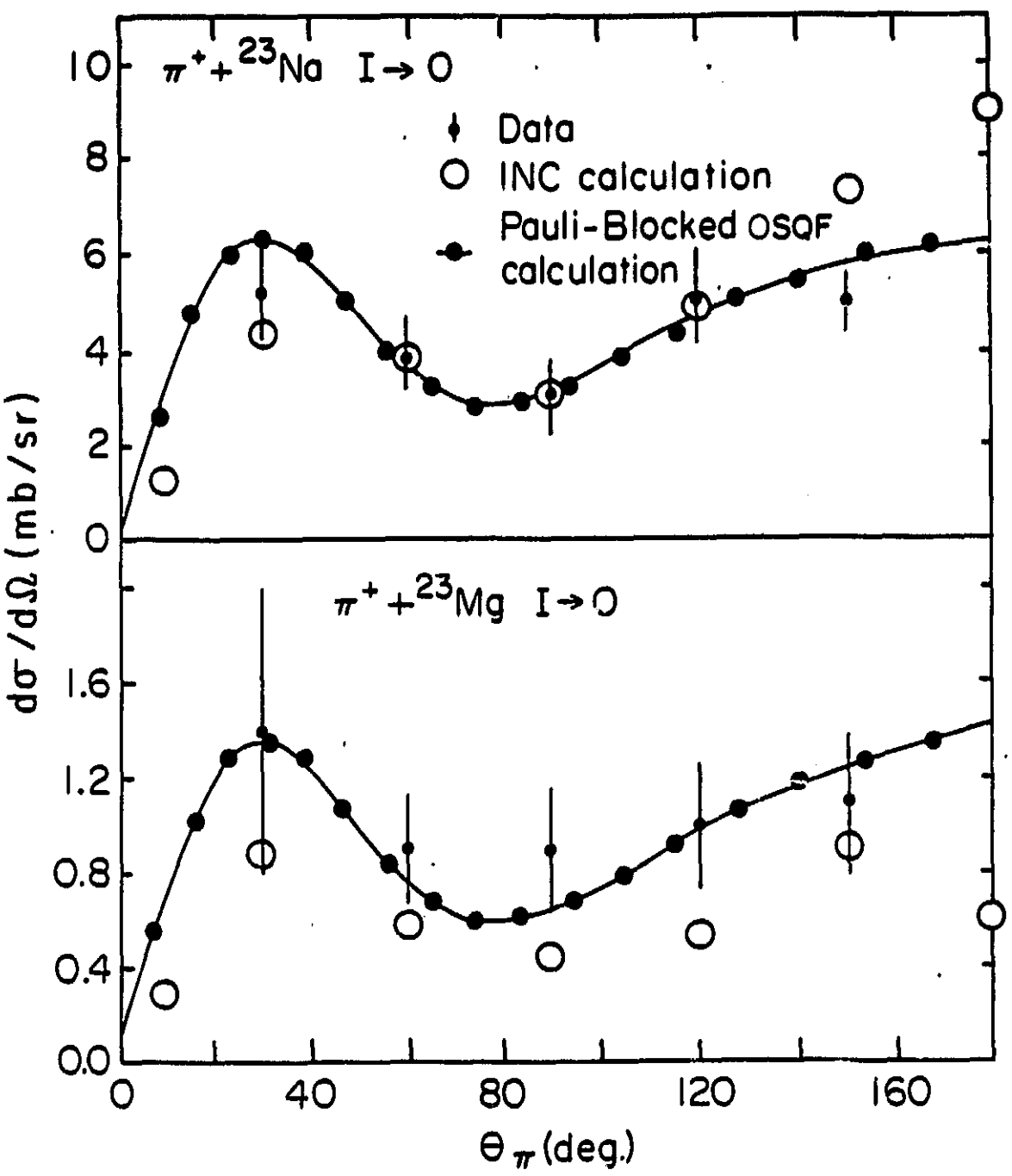
$\pi^+ + {}^{23}Na$ I → 0
Data
INC calculation
Pauli-Blocked OSQF calculation
$\pi^+ + {}^{23}Mg$ I → 0
dσ/dΩ (mb/sr)
Θ_π (deg.)
0
40
80
120
160
0.0
0.4
0.8
1.2
1.6
2
4
6
8
10

Fig. 5

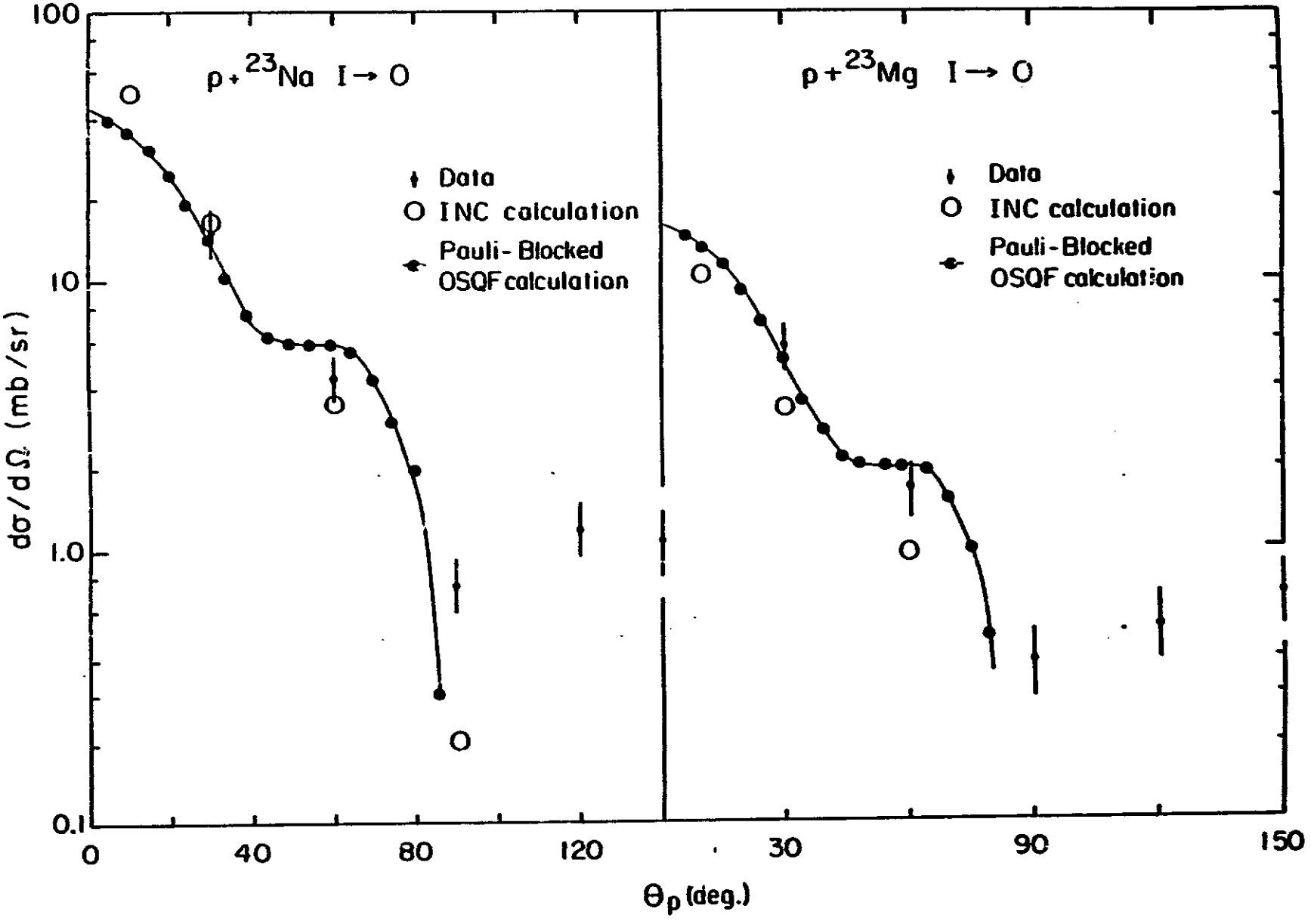
p + 23Na I → 0
Data
INC calculation
Pauli-Blocked OSQF calculation
p + 23Mg I → 0
Data
INC calculation
Pauli-Blocked OSQF calculation
dσ/dΩ (mb/sr)
100
10
1.0
0.1
0
40
80
120
30
90
150
θp (deg.)

Fig.6

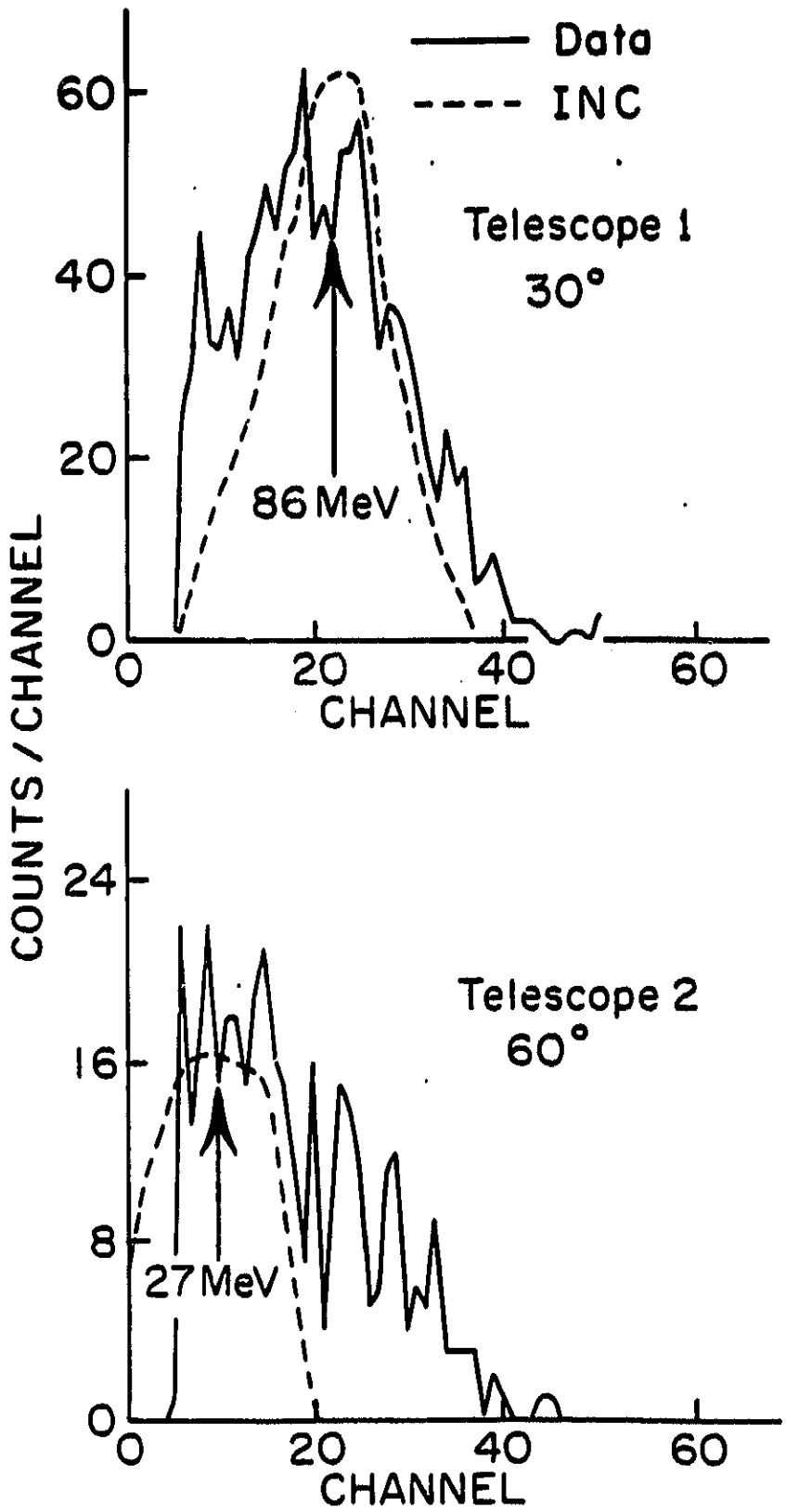
Data
INC
Telescope 1
30°
86 MeV
60
40
20
0
0
20
40
60
CHANNEL
COUNTS / CHANNEL
24
16
8
0
Telescope 2
60°
27 MeV
0
20
40
60
CHANNEL

Fig. 7

Table I. Experimental differential cross sections for $^{24}Mg(\pi,\pi N)$. $\sigma_\pi(^{23}Na)$ is the differential cross section for production of the ^{23}Na first excited state ($5/2^+$, 0.439 MeV) in coincidence with a π^+. Similar definitions apply for the other cross sections. Results are shown for each Ge(Li) and as an average which was weighted by the fractional errors. Telescope 1 was averaged with Telescope 6 for the 30° results.

Reaction	Telescope	Angle	Ge(Li) 1 $\left(\frac{mb}{sr}\right)$	Ge(Li) 2 $\left(\frac{mb}{sr}\right)$	Average $\left(\frac{mb}{sr}\right)$
$\sigma_\pi(^{23}Na)$	1	30°	7.3±1.9	4.6±1.2 }	5.2±1.1
	6	30°	4.8±1.3	1.9±1.3 }	
	2	60°	4.4±1.2	3.3±0.9	3.9±0.9
	3	90°	4.0±1.1	1.6±0.5	3.0±1.0
	4	120°	6.3±1.7	4.1±1.1	5.2±1.0
	5	150°	6.2±1.6	4.2±1.1	5.2±1.0
$\sigma_\pi(^{23}Mg)$	1	30°	1.5±0.5	1.9±0.5	1.4±0.5
	6	30°	1.4±0.5	0.31±0.15	
	2	60°	1.1±0.4	0.74±0.25	0.90±0.22
	3	90°	0.82±0.34	0.97±0.30	0.92±0.23
	4	120°	1.2±0.5	0.89±0.29	1.0±0.25
	5	150°	0.72±0.28	1.3±0.4	1.1±0.30
$\sigma_p(^{23}Na)$	1	30°	15.0±4.0	16.0±4.0 }	15.0±4.0
	6	30°	18.0±4.0	11.0±3.0 }	
	2	60°	4.8±1.3	4.0±1.1	4.4±0.9
	3	90°	0.59±0.28	0.85±0.30	0.76±0.20
	4	120°	1.5±0.5	0.87±0.31	1.2±0.3
	5	150°	1.3±0.5	0.45±0.20	0.93±0.27
$\sigma_p(^{23}Mg)$	1	30°	7.6±2.0	7.7±1.9 }	5.8±1.4
	6	30°	5.1±1.4	2.8±0.80 }	
	2	60°	2.1±0.7	1.3±0.4	1.7±0.4
	3	90°	0.48±0.24	0.31±0.15	0.39±0.14
	4	120°	0.45±0.25	0.59±0.25	0.54±0.18
	5	150°	0.93±0.38	0.28±0.15	0.69±0.22

Table II. Experimental and calculated angle-integrated absolute cross sections for $^{24}Mg(\pi^+,\pi N)^{23}Mg$ $(5/2^+, 0.450$ MeV) and $^{24}Mg(\pi^+,\pi^+p)^{23}Na(5/2^+, 0.439$MeV). σ_{OSQF} was calculated assuming nuclear Pauli blocking and nucleon occupation numbers given by C^2S^{-1} (see text).

Final Nucleus	Outgoing Particle	σ_{exp} (mb)	σ_{INC} (mb)	$\frac{\sigma_{exp}}{\sigma_{INC}}$	σ_{OSQF} (mb)	$\frac{\sigma_{exp}}{\sigma_{OSQF}}$
^{23}Na	π^+	52	32	1.6	263	0.20
	p	44	33	1.3	263	0.17
^{23}Mg	π^+	11	4.5	2.4	29	0.38
	p	16	6.5	2.5	58	0.28